

REPUBLIQUE ALGERIENNE DEMOCRATIQUE ET POPULAIRE

الجمهورية الجزائرية الديمقراطية الشعبية

MINISTRY OF HIGHER EDUCATION
AND SCIENTIFIC RESEARCH

HIGHER SCHOOL IN APPLIED SCIENCES
--T L E M C E N--



المدرسة العليا في العلوم التطبيقية
École Supérieure en
Sciences Appliquées

وزارة التعليم العالي والبحث العلمي

المدرسة العليا في العلوم التطبيقية
-تلمسان-

Mémoire de fin d'étude

Pour l'obtention du diplôme de Master

Filière : Électrotechnique
Spécialité : Energie et environnement

Présenté par : Mohammed Yacin MARKMAL

Thème

**Simulation numérique d'écoulements
d'air dans un canal rectangulaire muni
de chicanes au sein d'un capteur solaire**

Soutenu publiquement, le 11 / 07/ 2021, devant le jury composé de :

Dr. BOUDGHENE STAMBOULI Naouel Ep BENDIMERAD	MAA	ESSA-Tlemcen	Présidente
Dr. KORTI Mohamed Choukri	MCB	URER-MS ADRAR	Directeur de mémoire
Dr. KHERBOUCHE Djamila Ep FARADJI	MCA	ESSA-Tlemcen	Co-directeur de mémoire
Dr. BENNEKROUF Mohammed	MCB	ESSA-Tlemcen	Examineur
Dr. BOUKLI HACENE Souhila	MCB	Univ. de Tlemcen	Examineur

Année universitaire : 2020 / 2021

بِسْمِ اللَّهِ الرَّحْمَنِ الرَّحِيمِ

Acknowledgements

I want to thank the Almighty God for the strength, the will and capacity to carry out and persist and accomplish this job successfully.

I would like to thank my supervisors, **Mr Mohammed Choukri KORTI** and **Mrs Djamila KHERBOUCHE**, for their guidance, their assistance ,the precious time they gave me and their precious advices and useful critiques. Their skills and experience in the field have been of great help to me and i was really lucky to work with them during this period.

I am grateful to all the members of the jury for agreeing to read this manuscript and to provide the necessary critiques for the final form of this work.

Dedication

I dedicate this work..

To my family, the ones who made me the man I am.

To my heaven and the light of my eyes, my mother, who believed in me the most and taught me the meaning of life.

To my father, the hero who gave me the strength and encouraged me through the entire journey.

To Ali, The example that I always tried to follow his steps.

To all my brothers and sisters, who always surrounded me with their unconditional support through all their priceless advices.

To all my friends we s7ab, all my beloved ones and for everyone who helped me either directly or indirectly during my studies.

Mohammed Yacin MARKMAL

Abstract

The objective of this work is the numerical simulation of the thermal behaviour of a solar air collector (solar dryer). The low heat exchange between the heat transfer fluid and the absorber leads us to investigate other ways to improve the efficiency of the collector, for that it was very useful to study the geometrical shape, the dimensioning and the velocity that circulates inside the tubes. A 3D numerical model of a planar solar dryer, 94 cm long and 6 cm high, with a 3-part configuration for insulation, fluid flow and heating. The fluid is considered to be laminar with constant properties. The governing equations are the Navier-Stokes equations, coupled with the energy conservation equation solved using the commercial code (ANSYS FLUENT). The study examines the influence of inlet velocity and ambient temperature on the air temperature profiles to select the best possible performance for the model under study.

ملخص

الهدف من هذا العمل هو المحاكاة العددية للسلوك الحراري لمجمع الهواء الشمسي (المجفف الشمسي) . يقودنا التبادل الحراري المنخفض بين مائع نقل الحرارة والممتص إلى استكشاف طرق أخرى لتحسين كفاءة المجمع، لذلك كان من المفيد جدا دراسة الشكل الهندسي والأبعاد والسرعة التي تدور داخل الأنابيب. نموذج رقمي ثالثي الأبعاد لمجفف شمسي مستو، بطول 94 سم وارتفاع 6 سم، مع تكوين من 3 أجزاء للعزل وتدفق السوائل والتدفئة. يعتبر المائع صفيحيًا بخصائص ثابتة. المعادلات الحاكمة هي معادلات Navier-Stokes ، مقترنة بمعادلة الحفاظ على الطاقة التي تم حلها باستخدام الكود التجاري (ANSYS FLUENT). تبحث الدراسة في تأثير سرعة المدخل ودرجة الحرارة المحيطة على ملامح درجة حرارة الهواء الاختيار أفضل أداء ممكن للنموذج قيد الدراسة.

Résumé

L'objectif de ce travail porte sur la simulation numérique du comportement thermique d'un capteur solaire à air (séchoir solaire). Les faibles échanges thermiques entre le fluide caloporteur et l'absorbeur nous ramènent à investiguer d'autres moyens pour améliorer le rendement du capteur, pour cela, il a été très utile d'étudier la forme géométrique, le dimensionnement et la vitesse qui circule à l'intérieur des tubes. Un modèle numérique en 3D d'un séchoir solaire plan, de longueur 94 cm et de hauteur 6 cm, avec une configuration de 3 parties pour l'isolation, la circulation du fluide et l'échauffement. Le fluide est considéré comme laminaire avec des propriétés constantes. Les équations qui gouvernent l'écoulement sont celles de Navier-Stokes, couplées à l'équation de conservation d'énergie résolue à l'aide du code commercial (ANSYS FLUENT). L'étude examine l'influence de la vitesse d'entrée et de la température ambiante sur les profils de la température d'air pour choisir le meilleur rendement possible au modèle étudié.

Contents

1	Literature Review	3
1.1	The Sun	3
1.1.1	Structure of the Sun	4
1.2	Earth Characteristics	5
1.2.1	The terrestrial atmosphere	5
1.3	Earth's Movement	5
1.3.1	Earth's Movement Around the Sun	5
1.3.2	The Apparent Motion Of The Sun	6
1.3.3	The Celestial Sphere	7
1.4	Solar Energy	7
1.4.1	Specific Characteristics Of Solar Energy	8
1.5	The Position Parameters	9
1.5.1	The geographical coordinates of a site	9
1.5.2	The coordinates of the sun relative to an observer	9
1.6	Solar times	14
1.6.1	True solar time (Tsol)	14
1.6.2	Mean Solar Time (MST)	14
1.6.3	Universal Time (UT)	15
1.6.4	Legal time (LT)	15
1.6.5	Sunrise and sunset	15
1.6.6	The length of the day	16

1.7	Solar radiation	16
1.7.1	The spectrum of solar radiation	17
1.7.2	Solar radiation	17
1.7.3	Attenuation of solar radiation (role of the atmosphere)	18
1.7.4	Sunshine rate	19
1.7.5	The solar potential in Algeria	19
1.8	Modes of Heat Transfer	20
1.8.1	Conduction	21
1.8.2	Convection	21
1.8.3	Radiation	21
1.9	SOLAR COLLECTORS	22
1.9.1	Definition and working principle of a flat plate solar collector	23
1.9.2	The different types of solar collectors	23
1.9.3	The main components of a glazed flat plate collector	27
1.9.4	How does a flat plate collector work	30
1.9.5	Parameters characterising the operation of a flat plate collector	31
1.10	Applications of flat plate solar collectors	32
1.10.1	Domestic water heating	32
1.10.2	Room heating	32
1.10.3	Indirect drying of agricultural products	33
2	mathematical modeling	35
2.1	Introduction	35
2.2	Setting up the problem into equations :	36
2.2.1	Continuity equation :	36
2.2.2	Momentum equation :	37
2.2.3	Energy equation :	37
2.2.4	Flow regimes : Laminar and turbulent	38
2.3	Principle of the finite volume method:	39
2.3.1	Description of a control volume	40

2.4	Subdivision of the study domain (mesh)	41
2.4.1	STRUCTURED MESHES	42
2.4.2	UNSTRUCTURED MESHES	46
2.4.3	MIXED MESHES	46
2.4.4	General mesh generation techniques	47
2.4.5	Mesh quality	47
2.5	Discretisation by the finite volume method	48
2.5.1	Discrete equations	48
2.6	Conclusion	50
3	Problem's position	51
3.1	Introduction	51
3.2	Physical model	53
3.3	Mathematical formulation	56
3.3.1	Simplifying assumptions	56
3.3.2	Steps involved in creating the sensor geometry :	57
3.4	Mesh	57
3.5	Boundary conditions	60
3.5.1	Initial conditions	60
3.5.2	Definition of the regions	61
3.5.3	Definition of boundary conditions :	63
3.5.4	Mesh exportation :	65
3.5.5	Calculation Preparation Steps in FLUENT:	65
3.6	Gambit and Fluent simulation tools	71
3.6.1	Gambit	71
3.6.2	Fluent code	74
3.7	conclusion	77
4	Results and discussion	78
4.1	Introduction	78

4.2	Results and discussion	79
4.2.1	Evolution of air temperature profiles for different inlet velocities	79
4.2.2	Evolution of air temperature profiles during the day	83
4.3	Conclusion	93

List of Figures

1.1	sectional view of the sun. [1]	4
1.2	Earth's orbit around the sun. [2]	6
1.3	apparent motion of the sun [3]	6
1.4	The Celestial Sphere [4]	7
1.5	Illustration of geographic latitude and longitude of the earth [5]	9
1.6	Variation of the declination angle δ throughout the year [6]	10
1.7	Horizontal frame of reference [6]	11
1.8	Solar altitude angle [7]	12
1.9	sun's azimuth [6]	13
1.10	Orientation of a solar collector [6]	13
1.11	Modeling of sunset and sunerise time in algeria [8]	16
1.12	Solar spectrum outside the atmosphere [9]	17
1.13	Solar radiation types [6]	17
1.14	Attenuation of solar radiation as it passes through the atmosphere [6]	19
1.15	Solar radiation potential in algeria [10]	20
1.16	Classification of solar collectors [11]	22
1.17	A flate plate solar collector [12]	23
1.18	A Flat plate collectors without glazing [12]	24
1.19	Water collector [13]	25
1.20	air collector [11]	25
1.21	Evacuated-tube collectors [12]	26
1.22	Line focus concentrator [12]	26

1.23	Point focus concentrator [12]	27
1.24	Cross section of a flate plate [14]	28
1.25	Flate plate collector [15]	30
1.26	Conventional solar water heating system [2]	33
1.27	Room heating system [16]	33
1.28	Utilization of Solar Air Collectors for Product's Drying Processes [17]	34
2.1	the transition from the laminair to the turbulent regime: the reynlods experience [18]	38
2.2	visualisation of a turbulent flow [19]	39
2.3	structured mesh	40
2.4	schematic representing a two-dimensional control volume	41
2.5	Examples of the structured (left) and unstructured mesh (right)	41
2.6	regular cartesian grid	42
2.7	irregular cartesian grid	43
2.8	Transformation from physical domain to computational domain	44
2.9	BLOCK STRUCTURED GRID	44
2.10	refined mesh (left) and different mesh (right)	45
2.11	chimera grid	45
2.12	unstructured triangle mesh	46
2.13	mixed mesh with non-conforming interface	47
2.14	the principle of staggered meshing	48
2.15	staggring meshing figure's symboles definition	48
2.16	control volume around the node p (one-dimensional case)	50
3.1	cross section of the collector with dimensions	54
3.2	a view from above on the collector dimensions	54
3.3	suggested collector design using Gambit	57
3.4	mesh commande button	58
3.5	volume commande button	58

3.6	mesh commande button	58
3.7	definition of the mesh parametrs	59
3.8	a view of the collector's hexahedral mesh	59
3.9	side view of the collector's hexahedral mesh	60
3.10	boundary conditions definition	60
3.11	upper region of the collector	61
3.12	lower region of the collector	62
3.13	central region of the collector	62
3.14	Glass as defined in gambit	63
3.15	Absorber as defined in gambit	63
3.16	inlet as defined in gambit	64
3.17	outmet as defined in gambit	64
3.18	mesh exportation	65
3.19	Scale verification	66
3.20	definition of model parameters	66
3.21	establishing the energy equations	66
3.22	chosing « laminar » as a flow regime	67
3.23	defining the radiation parameters of the model	67
3.24	definition of a new material	68
3.25	Setting boundary conditions	69
3.26	Setting the velocity inlet value	69
3.27	Setting the inlet temperature	69
3.28	Solution initialization	70
3.29	Starting calculations	70
3.30	Gambit's interface	71
3.31	operation tool window	72
3.32	geometrie construction window	72
3.33	geometrie generation window	73
3.34	boundary conditions definition buttons	73

3.35	tools buttons	73
3.36	global control window	74
3.37	Fluent launcher window	75
3.38	Fleunt interface	76
4.1	Evolution of the (X, Z)-temperature profiles of the air for an inlet velocity of 0.3 m/s.	80
4.2	Evolution of the (X, Z)-temperature profiles of the air for an inlet velocity of 0.1 m/s.	81
4.3	Evolution of the (X, Z)-temperature profiles of the air for an inlet velocity of 0.08 m/s.	82
4.4	Evolution of the (X, Z)-temperature profiles of the air for an inlet velocity of 0.05 m/s.	83
4.5	Evolution of the (X, Z)-air temperature profiles for an inlet velocity of 0.05 m/s at 08:00 ($T_{amb} = 274.75 \text{ K}$, $D_i = 189 \text{ W/m}^2$, $DH = 7 \text{ W/m}^2$) . . .	84
4.6	Evolution of the (X, Z)-air temperature profiles for an inlet velocity of 0.05 m/s at 10 h 00 ($T_{amb} = 278,95 \text{ K}$, $D_i = 922 \text{ W/m}^2$, $DH = 49 \text{ W/m}^2$) .	85
4.7	Evolution of the (X, Z)-air temperature profiles for an inlet velocity of 0.05 m/s at 12 h 00 ($T_{amb} = 285, 95$, $D_i = 1025 \text{ W/m}^2$, $DH = 60 \text{ W/m}^2$) .	86
4.8	Evolution of the (X, Z)-air temperature profiles for an inlet velocity of 0.05 m/s at 13 h 30 ($T_{amb} = 289, 95$, $D_i = 1044 \text{ W/m}^2$, $DH = 60 \text{ W/m}^2$) .	87
4.9	Evolution of the (X, Z)-air temperature profiles for an inlet velocity of 0.05 m/s at 14 h 00 ($T_{amb} = 291, 05$, $D_i = 1037 \text{ W/m}^2$, $DH = 60 \text{ W/m}^2$) .	88
4.10	Evolution of the (X, Z)-air temperature profiles for an inlet velocity of 0.05 m/s at 16 h 15 ($T_{amb} = 293,15 \text{ K}$, $D_i = 903 \text{ W/m}^2$, $DH = 55 \text{ W/m}^2$) .	89
4.11	Evolution of the (X, Z)-air temperature profiles for an inlet velocity of 0.05 m/s at 20 h 00 ($T_{amb} = 286,75 \text{ K}$, $D_i = 0 \text{ W/m}^2$, $DH = 0 \text{ W/m}^2$) . . .	90
4.12	Distribution of the temperature evolution on the solar collector box at 12:00	91
4.13	Inlet at 12:00	92

4.14 outlet at 12:00	92
--------------------------------	----

List of Tables

3.1	symbols and units for collector dimensions	55
3.2	collector's dimensions	55
3.3	Physical properties of materials used in the simulation	55
3.4	suggested velocities	60
3.5	different parameters of the 5th of january 2020 obtained from the URER- MS daily archive.	61

Nomenclature

A	Area of the wing	m^2
L	Length of the box	cm
H	Box height	cm
W	Width of the box	cm
D	Diameter of the main tubes	cm
T_{amb}	Ambiente temperature	K
D_i	Direct solar irradiation	W/m^2
D_H	Diffuse solar irradiation	W/m^2
d	Diameter of the two secondary tubes	cm
w	Distance between two secondary tubes	cm

General Introduction

Since the dawn of creation, people have tried to put solar radiation to use. The advancement of knowledge of radiation and in the design of technical devices for its collection and conversion has marked the scientific and industrial development of societies. The various solar technologies are now at different stages of development, from research to industrial implementation and market penetration.

Today, the technologies developed concern the collection of solar gains through bioclimatic architecture, the production of low temperature heat for the housing and tertiary sectors, etc.

These techniques can provide a certain number of energy services in place of conventional energy: hot water supply, space heating. They can also provide an energy service where other energies do not: isolated sites, rural areas in developing countries.

Among the renewable energies, solar energy is the most dominant and also the most easily exploitable. Because of the diversity of its use and the interest it has aroused throughout the world, this form of energy has experienced a great expansion in recent years. However, the high price of this energy compared to non-renewable energies is a handicap to the expansion of its use.

The optimisation of solar devices is among the recommended solutions to reverse the current trend and see the use of solar energy spread further around the world, which is why this study was aimed at studying the thermal behaviour of a solar collector designed for solar drying, which will give us useful information if we want to focus

on the optimisation of this device.

The work has been structured in the following way:

- A general introduction presenting the aim of the work and showing the interest of the numerical study.
- The second chapter presents the generalities on solar thermal storage as well as the bibliographical research carried out on the various analytical, numerical and experimental works on solar energy storage systems in relation to the treated subject.
- The third chapter is based on the mathematical modelling of the theoretical problem and a brief description of the finite volume method.
- The fourth chapter is devoted to the problem position with descriptions of the software Fluent and Gambit as well as the numerical simulation steps using the calculation code FLUENT. -The fifth chapter presents the different results obtained and their interpretations.
- At the end, a conclusion summarises the critical analysis of the results obtained.

Chapter 1

Literature Review

1.1 The Sun

The sun is a small star in the universe that is nearest to the earth and is located at the middle of a solar system. The sun has a pseudo-spherical form, similar to a massive ball of extremely hot gas made up of 80% hydrogen and 19% helium, with the remaining 1% made up of a combination of over 100 elements, nearly all known chemical elements [20, 21].

The sun is the origin of all energy sources on earth. This is true as well for non-renewable energies of fossil origin, such as hydrocarbons which are the result of photosynthesis; as for renewable energies, such as solar energy, geothermal energy, biomass...etc. [20, 21].

Comparable to a huge ball of very hot gas, the sun is a dwarf star with a pseudo-spherical shape that consists mainly of 80 % hydrogen and 19% helium, the remaining 1% being a mixture of over 100 chemical elements, Although the sun is a medium-sized star, it alone accounts for 99.9% of the mass of the solar system, which is dominated by the gravitational effects of the sun's large mass.

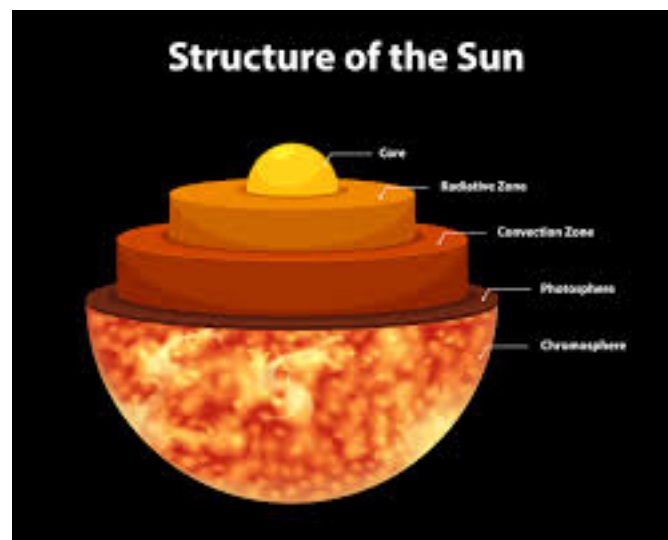


Figure 1.1: sectional view of the sun. [1]

1.1.1 Structure of the Sun

The sun is not a homogeneous sphere, it consists of 5 main areas: the interior, the photosphere, the chromosphere and the solar corona, the solar protuberances.

The interior : The interior contains the core, the radiation zone and the convection zone, it represents the energy source of the sun, it is composed of 2/3 of hydrogen and 1/3 of helium. The temperature reaches 16MK.

The photosphere : It is the gaseous layer that envelops the sun, it is responsible for almost all the radiation that the earth receives.

Chromosphere : It surmounts the photosphere, it is a gaseous layer that is assimilated to the solar atmosphere, its thickness does not exceed 800 (km) and its temperature is $43 \times 10^3 K$.

The corona : It is an irregular white halo without defined limits, its thickness is about $3 \times 10^6 km$ [22].

The solar protuberances : One of the most spectacular phenomena in the corona is the formation of protuberances. These are gigantic columns of gas, less hot but

denser than that of the corona, which are created near the surface and can extend over hundreds of thousands of kilometers.

1.2 Earth Characteristics

The main characteristics are given in table :

1.2.1 The terrestrial atmosphere

The atmosphere is made up of several layers, among which are: The troposphere is the region between the earth's surface and 15 kilometers above sea level.

The stratosphere is located between 15 and 80 kilometers above sea level.

The ionospheric zone , located between 80 and 200 kilometers above sea level.

1.3 Earth's Movement

1.3.1 Earth's Movement Around the Sun

The Earth's orbit around the Sun is an ellipse, with the Sun as one of the foci. The plan of this ellipse is known as the ellipsis. This ellipse has a low eccentricity.

The complete revolution takes place in a period of 365.25 days. The earth also turns on itself around an axis called the axis of the poles. This rotation takes place in one day. The axis of the poles and the ellipsis make an angle between them called declination, it is equal to $23^{\circ}27'$.

It is at the winter solstice (December 21) that the earth is closest to the sun: 147 million km.

On June 21, the distance between the earth and the sun is 152 million km, this is the day when the earth is the farthest away, it is the summer solstice.

March 21 and September 21 are called respectively spring and autumnal equinoxes. At the equinoxes the day and the night are equal.

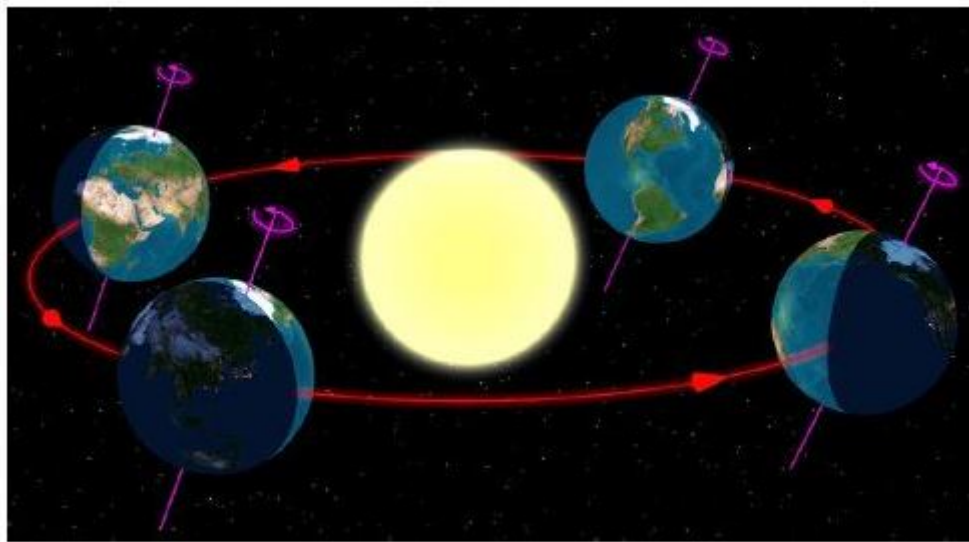


Figure 1.2: Earth's orbit around the sun. [2]

1.3.2 The Apparent Motion Of The Sun

The movement that the Sun appears to make in a day seen by an observer located on Earth is called "The apparent motion of the Sun". Outside of the polar regions, the the Equator and the tropics. [3]

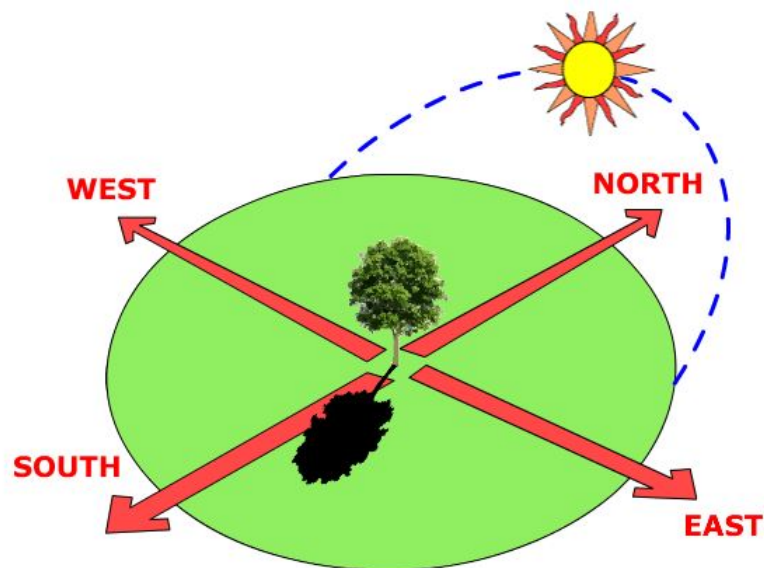


Figure 1.3: apparent motion of the sun [3]

-In the morning; the Sun is in the East, low on the horizon, it is the "Sunrise".

-At noon; the Sun is positioned in the South or in the North, and it is at the highest of its path apparent.

-In the evening; the Sun appears in the West, low on the horizon, it is the "sunset".

The apparent movement of the Sun observed by a fixed man at a point of latitude L north of the Equator is shown in figure 1.3.

1.3.3 The Celestial Sphere

The celestial sphere is a fictitious sphere with a huge diameter, which has as its center the earth, and as its radius the distance (earth-sun). It is assumed that all visible objects in the sky are located on the surface of the celestial sphere. The direction of the objects can be precisely evaluated with the help of a celestial coordinate system, We can summarize the different characteristics on the sphere itself as shown in figure 1.4.

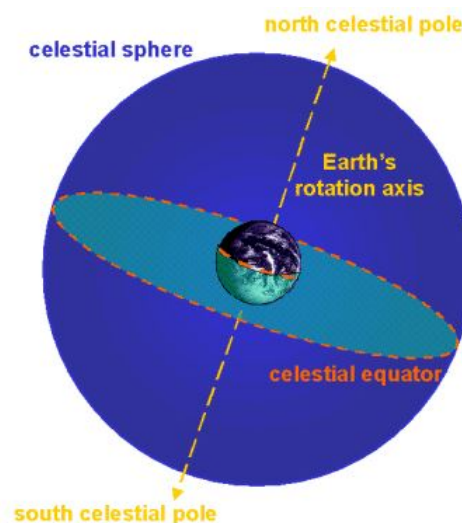


Figure 1.4: The Celestial Sphere [4]

1.4 Solar Energy

Solar energy is the energy emitted by the sun through its radiation on the earth can be converted into other forms of energy useful for human activity, such as heat, electricity, or biomass, by a variety of processes. Furthermore, the term "solar energy"

is sometimes used to refer to the electricity or thermal energy produced as a result of this [23].

Solar Photovoltaic Energy Photovoltaic solar energy refers to the electricity produced by transforming part of the sun's radiation with a photovoltaic cell.

Solar thermal energy Solar thermal energy consists of using solar radiation by transforming it into thermal energy. It is presented in different ways: thermodynamic solar power plants, solar water heaters and heating, solar cooling, solar stoves and dryers.

1.4.1 Specific Characteristics Of Solar Energy

Some particularities of solar energy must be taken into account to optimize its use, the main characteristics are dilution and intermittence.

Dilution : The dilution requires the use of a large surface of capture to obtain high powers or to provide a concentration of solar rays to obtain high temperatures.

Intermittency : The intermittency of solar radiation and the other Specific characteristics of solar energy, In temperate climate regions, the problem of intermittency is difficult to solve. A solution often used is to consider storage of very variable importance depending on the applications considered.

For example, it is necessary to plan a daily storage and to use it during the night, as well as to plan the nebulous storage which corresponds to accidental cloudy passages.

1.5 The Position Parameters

1.5.1 The geographical coordinates of a site

Every point on the earth's sphere can be located by two coordinates, called earth coordinates, namely latitude and longitude, figure 1.5:

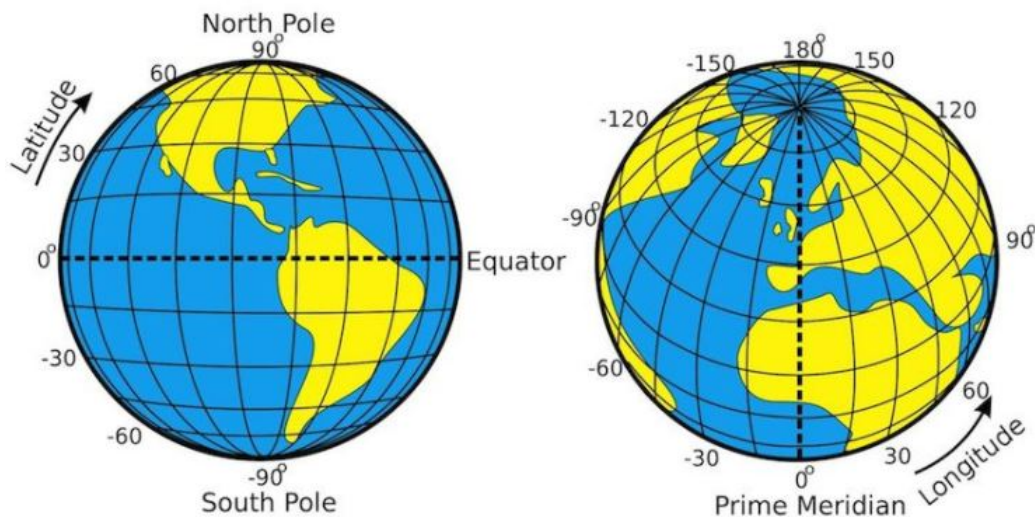


Figure 1.5: Illustration of geographic latitude and longitude of the earth [5]

The latitude of the location ϕ : This is the angle that the ray joining the center of the earth at this location and the equatorial plane. It varies from -90° at the South Pole to $+90^\circ$ at the North Pole:

$\phi < 0$ *The Southern Hemisphere.*

$\Phi > 0$ *The Northern Hemisphere.*

$\phi = 0$ *On the plane of the equator.*

The longitude of the location \mathbf{L} : This is the angle between the meridian plane passing through this location and the original meridian plane (Greenwich 0°).

1.5.2 The coordinates of the sun relative to an observer

To determine the coordinates of the sun relative to an observer located on the surface of the earth surface of the earth we define two reference frames, the equatorial frame

and the horizontal frame.

The equatorial reference frame

The equatorial frame of reference is a frame of reference that takes as its origin the center of the earth and as reference plane the plane of the equator. In this frame, the position of the sun in the sky is determined by two sky is determined by two coordinates, the declination and the hour angle [20].

The declination of the sun (δ) : Corresponds to the angle formed by the equatorial plane and the direction of the earth sun. It varies according to Cooper's equation, [20]:

$$\delta = 23.45 \cdot \sin((284 + Nd) \cdot (360/365)) \quad (1)$$

With, Nd : the number of the day of the year (January 1=1).

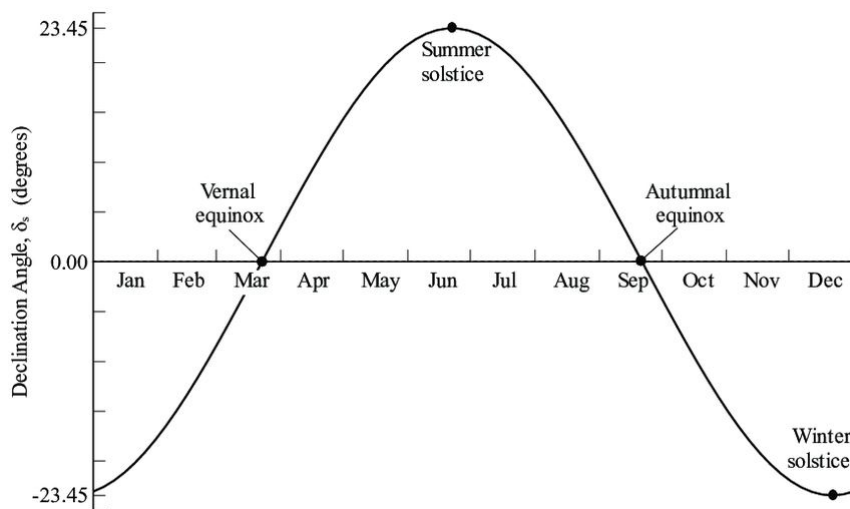


Figure 1.6: Variation of the declination angle δ throughout the year [6]

As we can see in figure 1.6 , it varies from $-23,45^\circ$ at the winter solstice to $+23,45^\circ$ at the summer solstice, and it is zero at the equinoxes

The hour angle (ω) : Corresponds to the angle between the projection of the sun on the equatorial plane and the meridian of the location under consideration passing through the south. It is given by the following relation:

$$\omega = 15.(T_{sol} - 12) \quad (2)$$

where, T_{sol} , is the true solar time.

The horizontal reference frame.

The horizontal frame of reference is a reference frame that takes the observer's location as its origin and the plane of the astronomical horizon as its reference plane. In this frame of reference. The position of a star in space can be identified by its horizontal coordinates defined on the celestial sphere in figure 1.7, namely the height of the sun h and its azimuth a .

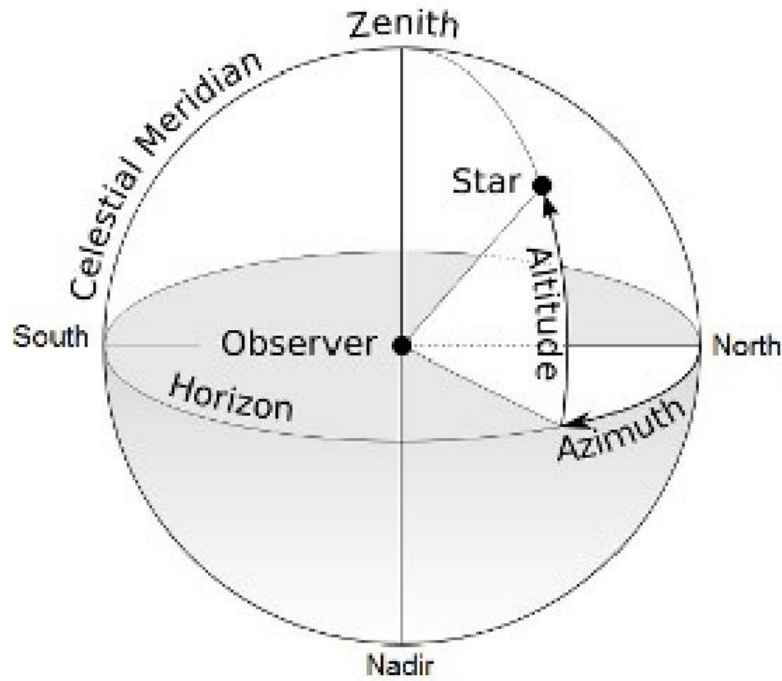


Figure 1.7: Horizontal frame of reference [6]

The height of the sun (h) It corresponds to the angle formed by the directional vector of the sun and its projection on the horizontal plane, figure 1.8, it is 0° at sunrise and sunset and takes its maximum value (90°) at solar midday . It is evaluated by the following relation [20] :

$$\sinh = \cos\delta.\cos\phi.\cos\omega + \sin\delta.\sin\phi \quad (3)$$

The maximum height of the sun corresponds to $\omega = 0$, obtained at midday in true solar time, and is evaluated by the following relation:

$$h_{max} = 90 - (\phi - \delta) \quad (4)$$

It varies with the latitude of a location and the declination of the sun (the day of the year). Figure (1-8) shows the evolution of the latter for different locations.

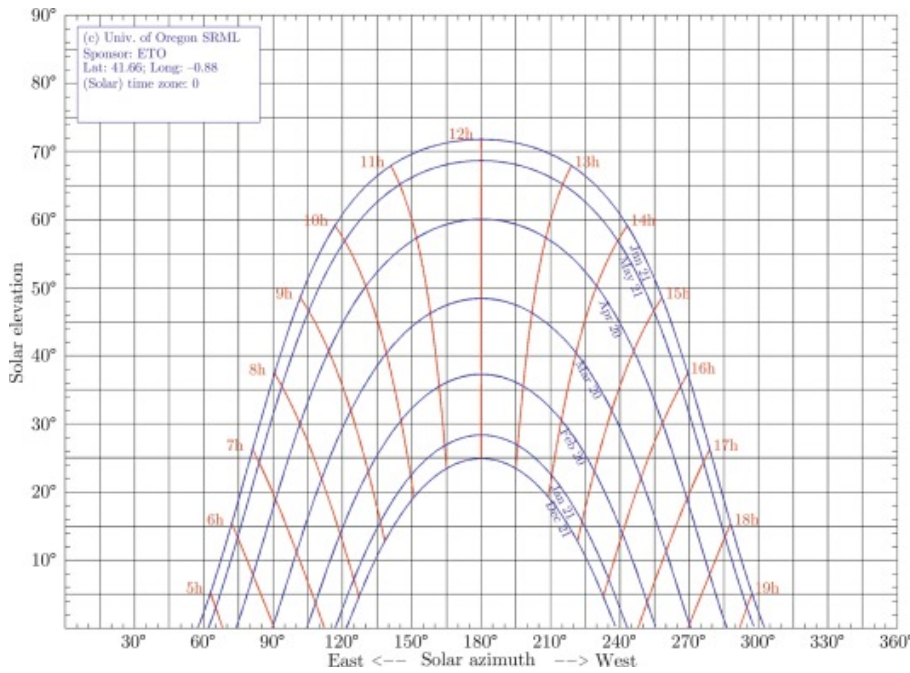


Figure 1.8: Solar altitude angle [7]

Sun's azimuth (a) This is the angle formed by the projection of the direction of the sun on the horizontal plane and the meridian of the location. It is counted positively towards the east and negatively towards the west. It is given by the following relation [20] :

$$\sin a = (\cos \delta \cdot \sin \omega) / \cos h \quad (5)$$

Orientation of a plane

In solar applications, the positioning of the surface of solar devices (e.g. flat plate collector) is essential. the following figure shows the orientation of a sensor with the main angles, the collector tilt (beta, β) and azimuth (gamma, γ) are positioned to reflect a site somewhere in the Northern Hemisphere. The Sun's position is described

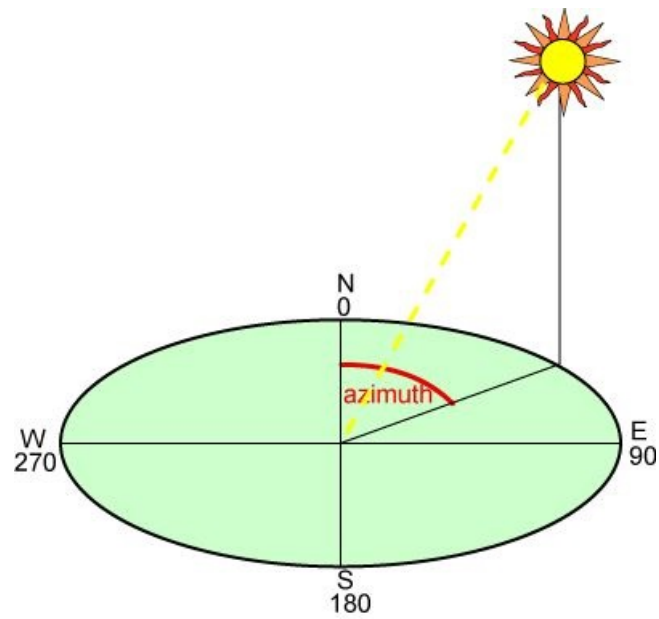


Figure 1.9: sun's azimuth [6]

fully using the solar altitude angle (α_s) and the solar azimuth angle (γ_s).

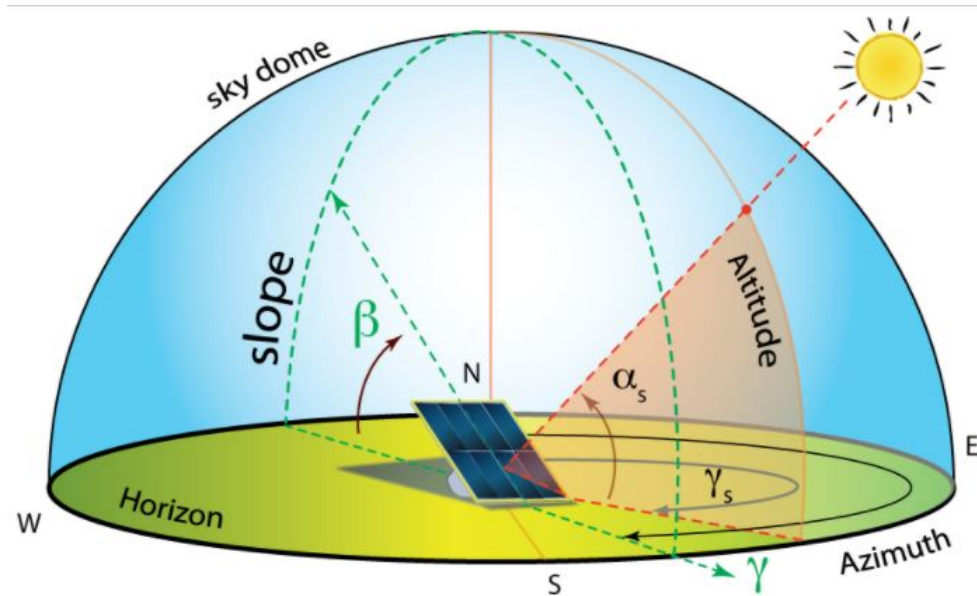


Figure 1.10: Orientation of a solar collector [6]

1.6 Solar times

1.6.1 True solar time (T_{sol})

The sun rotates in the plane of the equator by 360° in 24 hours, i.e. 15° per hour, so there is a simple relationship between the true solar time TSV and the hour angle ω [24].

$$\omega = 15.(T_{sol} - 12) \quad (6)$$

1.6.2 Mean Solar Time (MST)

The path of the earth around the sun is elliptical (Kepler's first law). During this motion, the Sun-Earth vector ray sweeps equal areas in equal times (Kepler's second law). All this, added to the fact that the Earth's axis of rotation is inclined to the ecliptic plane, means that the length of the true solar day varies according to the time of year[20].

We then introduce the notion of mean solar time (MST) which varies by $\pm 16mn$ with respect to true solar time (T_{sol}) which corresponds to the equation of time. MST is given by the following relation [24] :

$$MST = T_{sol} - ET \quad (7)$$

Where ET is the corrective term called the time's equation The sun rotates in the plane of the equator by 360° in 24 hours, i.e. 15° per hour, so there is a simple relationship between the true solar time TSV and the hour angle ω [24].

$$\omega = 15(T_{sol} - 12) \quad (8)$$

$$ET = -0.0002 + 0.4197\cos(0.984j) - 7.3509\sin(0.984j) - 3.2265\cos(20.984j) \\ - 9.3912\sin(20.984j) - 0.0903\cos(30.984j) - 0.3361\sin(30.984j) \quad (9)$$

1.6.3 Universal Time (UT)

Universal time is equal to the mean solar time of the prime meridian (Greenwich meridian). It is expressed as follows [1]:

$$UT = MST + \frac{L}{15} \quad (10)$$

with L: the longitude given in degrees and the times in hours.

1.6.4 Legal time (LT)

Legal time is the time we read on clocks and is given by the following relationship [1]:

$$LT = UT + C1 + C2 \quad (11)$$

With : C1 is the time difference from Greenwich Mean Time

C2 is summer and winter time, if applicable.

1.6.5 Sunrise and sunset

The hour angle at sunrise and sunset corresponds to $\omega = 0$, by replacing in formula (1.3), we find:

$$\omega_r = \arccos(-\tan\delta \cdot \tan\phi) \quad (12)$$

According to the relation (1.7) the solar time at sunrise has therefore the expression:

$$(T_{sol})_s = 12 - \frac{\omega_r}{15} \quad (13)$$

The hour angle ω_c at sunset is the opposite of the hour angle at sunrise, Therefore, $\omega_s = -\omega_r$, the solar time at sunset has the value :

$$(T_{sol})_s = 12 - \frac{\omega_s}{15} = \frac{\omega_r}{15} \quad (14)$$

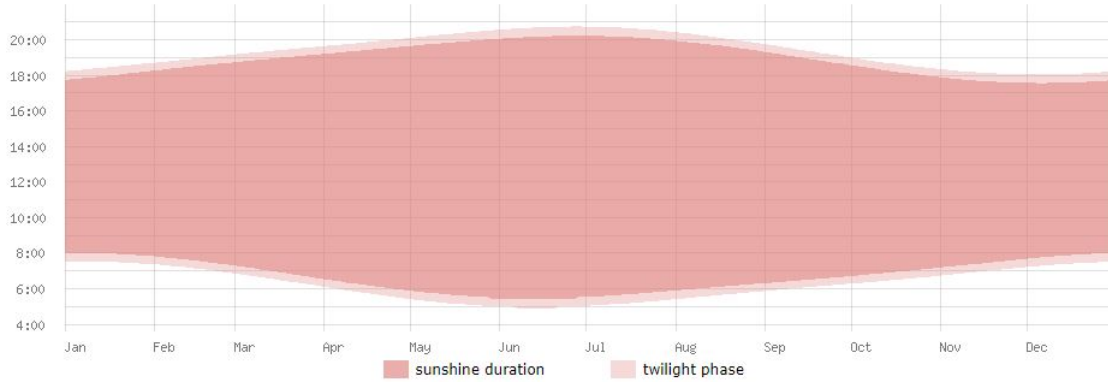


Figure 1.11: Modeling of sunset and sunrise time in Algeria [8]

1.6.6 The length of the day

The duration of the day is given by the following formula [24]:

$$d = (T_{sol})_s - (T_{sol})_r = 2x \frac{\omega_l}{15} \quad (15)$$

1.7 Solar radiation

The radiation emitted by the sun is the external manifestation of the nuclear interactions nuclear interactions that take place in the core of the sun and the set of secondary interactions that they generate in its envelope. This radiation constitutes almost all of the energy expelled by the sun [25].

The thermonuclear reactions produced in the core of the sun generate particle and electromagnetic radiation and electromagnetic radiation propagating in all directions in the vacuum with a speed of 3×10^8 m/s and covering all wavelengths from X-rays

and gamma rays to the far infrared. However 99.9% of the energy is between 0.2 and 0.8 μm .

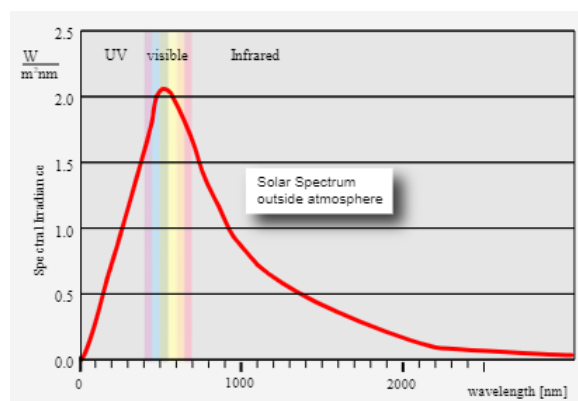


Figure 1.12: Solar spectrum outside the atmosphere [9]

1.7.1 The spectrum of solar radiation

The spectrum of solar radiation can be approximately divided into ultraviolet (UV), visible light, infrared (IR) and long wavelength (heat).

1.7.2 Solar radiation

solar radiation is the energy received over a certain period of time. It depends on several parameters such as: season, latitude and orientation of the receiving surface.

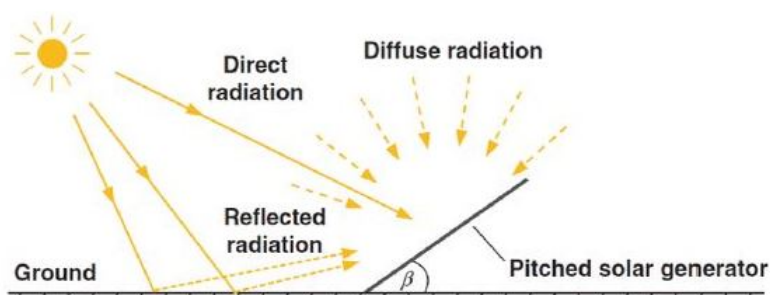


Figure 1.13: Solar radiation types [6]

Such radiation consists mainly of :

Direct radiation

is the radiation that passes through the atmosphere without undergoing it is received directly from the sun, without diffusion through the atmosphere, its rays are parallel to each other. are parallel to each other.

diffused radiation

is the part of the solar radiation scattered by solid or liquid particles suspended in the atmosphere. solid or liquid particles suspended in the atmosphere (air, clouds, aerosols, etc.). It does not have a preferred direction.

Global radiation is the sum of direct and diffused radiation.

The albedo

A part of the incident solar radiation is reflected by the atmosphere (mainly by clouds) and by the ground. This is the albedo flux [25].

It is the ratio of the solar energy reflected by a surface to the incident solar energy.

1.7.3 Attenuation of solar radiation (role of the atmosphere)

Solar energy is attenuated by various atmospheric components such as air molecules, aerosols, gases air molecules, aerosols, gases, cloudy water droplets or ice crystals suspended in the atmosphere ice crystals suspended in the atmosphere...

In fact , it undergoes transformations as it passes through the atmosphere by absorption and diffusion.

The absorption is selective and depends mainly on 4 elements, which are :

- Ozone which forms a screen and stops UV (<0.28m) harmful to life. Oxygen which absorbs narrow bands of the visible spectrum (around 0.69 and 0.76m).
- Carbon dioxide which absorbs part of the far IR (>2m). Water vapour which causes multiple absorption bands especially in the IR, it is found almost only at ground level (Z<5km).
- Dust and clouds are also important in the scattering of solar radiation.

The influence of atmospheric components on the spectral distribution

The influence of atmospheric components on the spectral distribution of direct and diffuse solar radiation can be seen in the following figure 1.14:

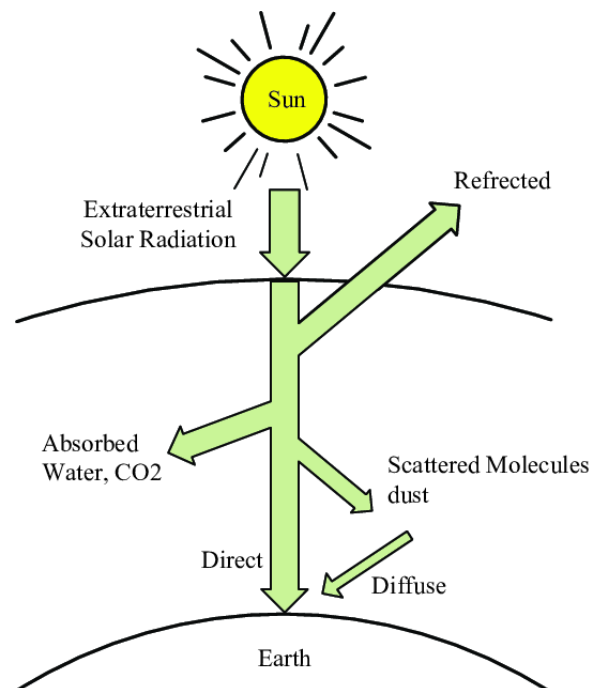


Figure 1.14: Attenuation of solar radiation as it passes through the atmosphere [6]

1.7.4 Sunshine rate

Under clear, cloudless skies, the ground receives direct solar radiation for the entire duration of the day, or more precisely for the maximum sunshine duration. The sunshine rate is defined as the ratio between the actual and the maximum sunshine duration.

1.7.5 The solar potential in Algeria

The solar potential is a set of data describing the evolution of available solar radiation over a given period. It is used to simulate the operation of a solar energy system and to make a dimensioning as exact as possible taking into account the demand to be met. Due to its geographically solar deposit as shown in Figure 1.15 :

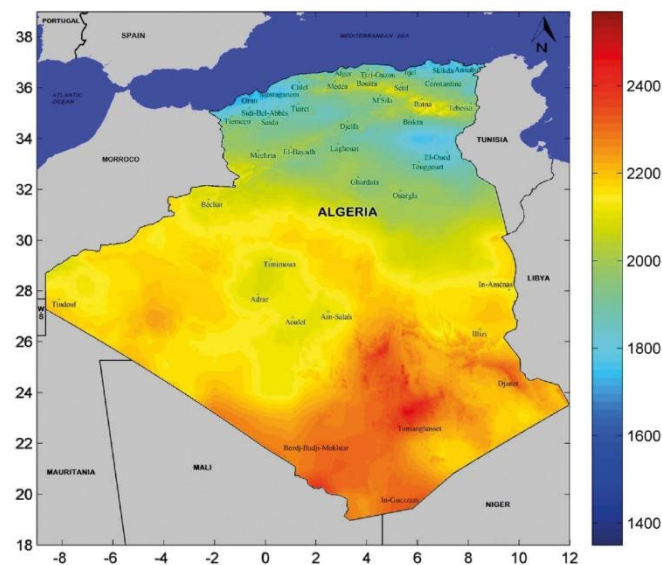


Figure 1.15: Solar radiation potential in Algeria [10]

Following a satellite evaluation, the German Space Agency (ASA) has concluded that Algeria has the largest solar potential in the Mediterranean region, i.e. 169,000 TWh/year for solar thermal, 13.9 TWh/year for solar photovoltaic. Algeria's solar potential is the equivalent of 10 large natural gas deposits that would have been discovered in Hassi R'mel [26]

The duration of insolation in the Algerian Sahara is of the order of 3500 h/year and is the highest in the world; it is always higher than 8 hours per day and can reach 12 hours per day during the summer, with the exception of the extreme south where it drops to 6 hours per day during the summer. The Adrar region is particularly sunny and has the greatest potential of all Algeria.

1.8 Modes of Heat Transfer

There is a total of 3 Modes of Heat transfer which is:

1. Conduction
2. Convection
3. Radiation

1.8.1 Conduction

In conduction, heat or energy is transmitted by physical interaction, such as when you touch a hot object with your palm. When we heat the iron on one side, the molecules contained in it migrate to the other side and heat the field as well. As a result, we can assume that Conduction is equivalent to Direct touch. It is known as the transfer of heat by molecular agitation within a material without the material as a whole moving [27].

Heat Conduction Rate Equations (Fourier's Law) :

Heat Flux :

$$q = -k \cdot \frac{dT}{dx} \quad (16)$$

k : thermal conductivity W/m.K

1.8.2 Convection

Heat or energy is transmitted by mass motion of a substance, such as air or water, as warm fluid is induced to travel away from the source of heat-carrying energy [27].

Heat Convection Rate Equations (Newton's Law of Cooling) :

Heat Flux :

$$q = h(T_f - T_s) \quad (17)$$

h : Convection Heat Transfer Coefficient W/m².K

1.8.3 Radiation

The Radiation is defined as Everybody emits radiation in the form of an electromagnetic wave or rays or particles. In this process does not require a medium to transfer the Thermal (Heat) energy [27].

Heat Radiation power :

$$E_b = e\sigma T^4 \quad (18)$$

e : emissivity ($0 \leq e \leq 1$)

σ : Stefan – Boltzmann's constant $W/m^2.K^4$

1.9 SOLAR COLLECTORS

Solar collectors are devices whose operating principle is based on the transformation of solar energy into heat. In what's next we will see the concept, the components and the types of a solar collector.

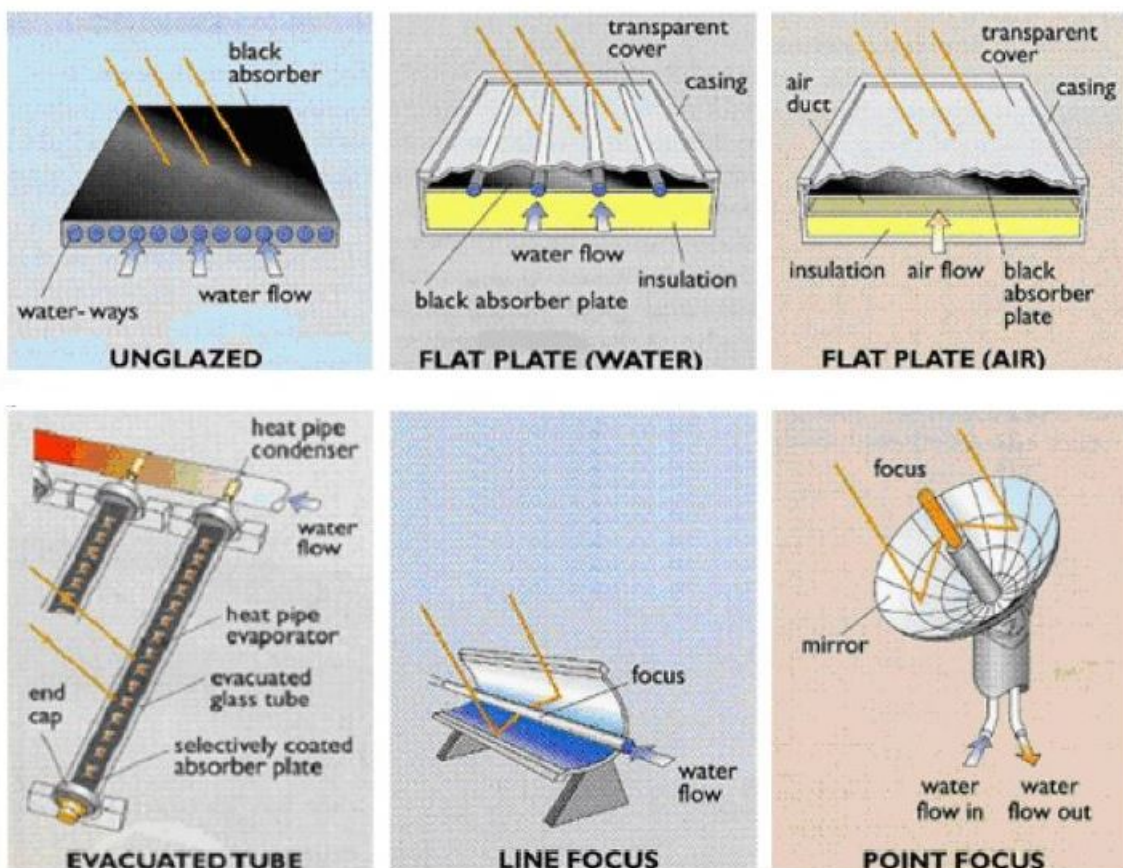


Figure 1.16: Classification of solar collectors [11]

1.9.1 Definition and working principle of a flat plate solar collector

A flat plate solar collector refers to all systems that are exposed to solar radiation in order to capture it and transform it into thermal energy. This collection system is based on the greenhouse effect where radiation is collected in the visible and near infrared range (wavelengths between 0.3 and 3 μm). This radiation passes through the glass of the sensor, where it is trapped inside, and then captured by the absorber surface. The absorber in turn emits thermal radiation in the far infrared range (between 4 and 30 μm). This radiation is completely stopped by the glass wall, which by the glass wall, which heats up and radiates half towards the absorber surface and half towards the outside. half towards the outside. The fluid that circulates under this wall (heat transfer fluid) recovers part of this absorbed energy by convection and undergoes a rise in temperature as it passes through [28].

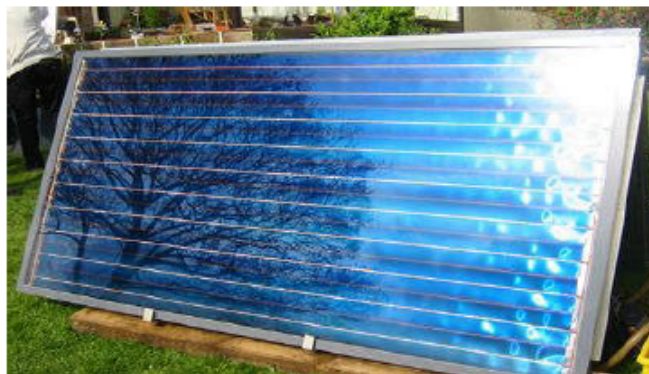


Figure 1.17: A flat plate solar collector [12]

1.9.2 The different types of solar collectors

In order to intercept the energy from solar radiation, there are several types of solar collectors. The following is a brief description of the five most common types of flat plate solar collectors.

Flat plate collectors without glazing

This is the simplest, most economical but least efficient model. It is usually made up of a simple metal or plastic plate (absorber) on which several tubes carrying the

heat transfer fluid are glued. Flat plate collectors unglazed flat plate collectors are not insulated on the front side, which is why they are better suited to applications at low temperatures (below 30°C). This type of collector is mainly used for heating outdoor swimming pools. Because they have no glazing, these collectors absorb a large proportion of the sun's energy. However, because they are not insulated on the front, much of the heat absorbed is lost when it is windy and the outside temperature is not high enough. The collectors are stirred by warm air and absorb the heat exchanged, especially during the night when the temperature is high and there is wind outside. The typical architectural integration of this type of product allows the implementation of a larger to compensate for the difference in efficiency with flat-plate glazed collectors, especially during the winter.



Figure 1.18: A Flat plate collectors without glazing [12]

flat-plate glazed collectors (water)

Flat-plate glazed solar collectors are very common. They are available as water collectors and air collectors. These collectors are best suited to moderate temperature applications where the desired temperatures are between 30°C and 70°C. Circulating water collectors are most commonly used for domestic hot water production on an individual or collective scale, for industrial use, and for indoor swimming pools.

Flat plate glazed collectors (air)

As their name indicates, they produce hot air. These collectors are used in some ventilation, soft ventilation and space heating systems. In the case of air heating, the air to be heated can be passed directly through the collector. through the collector. A



Figure 1.19: Water collector [13]

particular application of these collectors is the drying of certain agricultural products: hay, figs, apricots, etc. Note that these solar systems are light and have no cooling or boiling problems, which is an advantage over liquid collectors. Air collectors are used for drying, space heating and ventilation air. ventilation air.

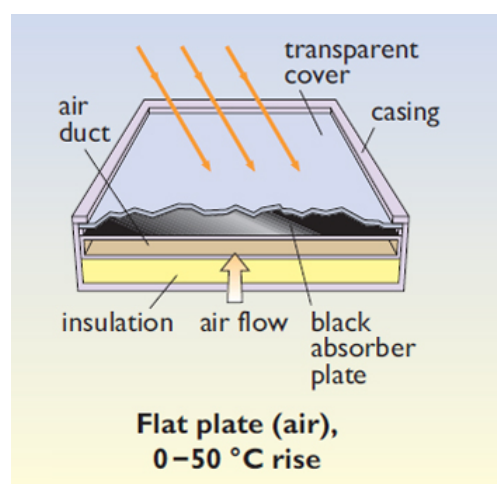


Figure 1.20: air collector [11]

Evacuated-tube collectors

Evacuated-tube solar collectors consist of a series of transparent glass tubes. In each tube there is an absorber plate to collect the solar radiation and an exchanger to help transfer the heat energy. The tubes are evacuated to prevent convective heat loss from the absorber plate and the absorber plate is selectively treated to prevent the radiation from dissipating in the form of long wave radiation. Thus, efficient solar collectors can be realized without solar collectors can be realised without the need for

additional thermal insulation or a protective casing.



Figure 1.21: Evacuated-tube collectors [12]

Line focus concentrators

This type of solar concentrators use parabolic or parabolic-cylindrical reflecting surfaces (mirrors) (figure III.9) to concentrate the sun's rays in the point or linear focus of these surfaces respectively. In the point focus or along the linear focus are the receivers (absorbers) that capture the concentrated solar heat. Naturally, these concentrators must follow the movement of the sun.



Figure 1.22: Line focus concentrator [12]

Point focus concentrators

These collectors use parabolic reflective surfaces to concentrate the sun's rays in the focalpoint where the absorber is located to capture the concentrated solar heat . The idea of using a parabolic surface comes from the fact that it is stigmatic (gives at the exit of the parabola a beam converging in a point) for the points at infinity located

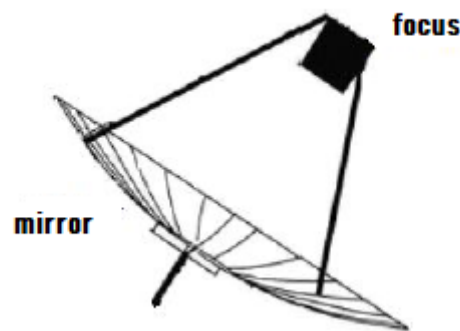


Figure 1.23: Point focus concentrator [12]

on its axis. According to the laws of reflection, any light ray parallel to the axis of the parabola is reflected by the parabola along a straight line passing through the focus. Thus the parabola focuses all reflected rays at a point called the "focus". This implies that these concentrators must follow the movement of the sun. Parabolic reflector systems can reach higher temperatures (up to 1500°) on the absorber. [29].

1.9.3 The main components of a glazed flat plate collector

A glazed flat plate collector consists mainly of a transparent cover (glazing), an absorber and thermal insulation, as shown in the next figure :

The transparent glass cover

Because of its resistance to mechanical aggression (impact, hail, snow, etc.) and thermal aggression (sudden cooling, etc.), safety glass is especially used as a transparent cover. In order to be as transparent as possible and transmitting solar radiation, it is preferable that the glazing is low in iron oxide. For roof-integrated collectors, synthetic materials are sometimes used. They are lighter, cheaper and easier to install, but have a shorter life span than ordinary glass. More often, the glazing is slightly structured, so that it spreads the reflected fraction of the incident solar radiation, to reduce possible glare. The main characteristics of a glazing are :

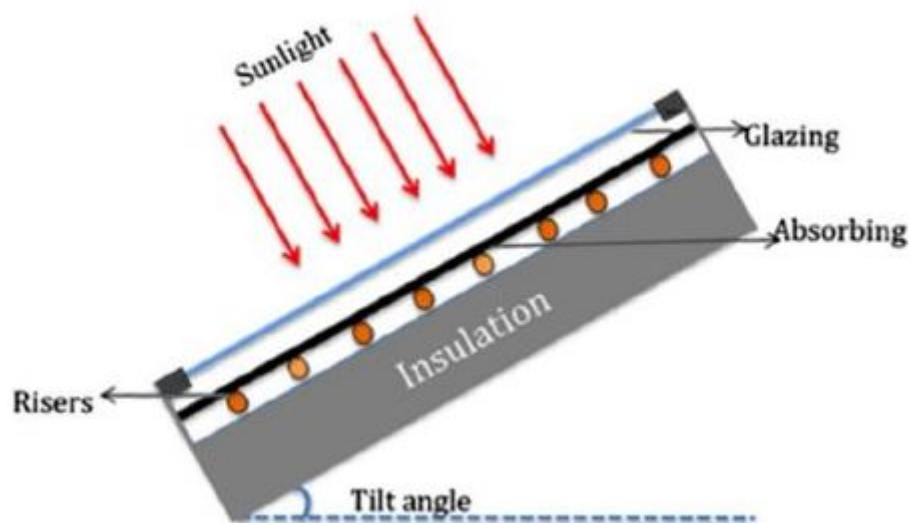


Figure 1.24: Cross section of a flat plate [14]

-Its transmission coefficient

-Its emission coefficient

The special feature of good glass is that it absorbs little solar radiation and therefore transmits the maximum amount of energy to the absorber. Currently, the most common glass used for flat collectors is prismatic glass. Its specificity is its low reflection of radiation (1.5%). It can transmit up to 96% of the radiation.

The absorber

The main role of an absorber is to capture solar radiation and convert it into heat energy. It is usually painted black to absorb all radiation in the visible, ultraviolet and a small amount of infrared radiation. infrared spectrum.

The absorber is chosen according to the following characteristics:

- A good absorption coefficient.
- A Good thermal conductivity.
- A Good corrosion resistance.

The choice of material and the construction process have a great influence on the quality of a sensor. Due to their high conductivity, copper, steel and aluminium are the most commonly used materials. are the most commonly used materials. In order

to reduce radiation losses, absorbers are usually coated with a selective layer. Nickel and chromium are the main metals used for selective for selective coatings for most collectors.

The heat transfer fluid

To remove the heat stored by the absorber plate, either air or water is generally used as the heat transfer fluid. Compared to water, air has the following advantages:

- It does not have problems with freezing in winter or boiling in summer.
- Dry air has no corrosion problems.
- There is no air leakage problem.
- There is no need to use a heat exchanger in the case of space heating.

The system to be implemented is simpler and more reliable.

The use of air instead of water has the following disadvantages:

- Air can only be used for space heating.
- The pipes must have a large cross-section to allow sufficient flow.
- Heat transfer is less good than with water.

In the case of pipes welded to the back of the absorber plate, care must be taken with the welds to reduce the risk of care must be taken with the welds to reduce the thermal contact resistance as much as possible resistance [20].

Insulation

A collector must be well insulated with suitable materials. These materials should have a low thermal conductivity to minimise heat loss by conduction through the conduction through the faces of the collector. Typically, the thickness of The thickness of the insulation is usually in the order of 5 to 10 cm. Mineral wools, synthetic materials (glass wool, expanded foams, etc.) are used. glass wool, polyurethane foam or polystyrene) are generally the insulating materials used. insulating materials used. They must be able to withstand the high temperatures that can be reached inside a collector. For an optimal choice of an insulating material, the following parameters should be considered:

- Density
- Maximum operating temperature
- Resistance to fire, rodents and rot
- Sensitivity to moisture
- Its cost

Frame

The enclosure, commonly made of aluminium or wood, encloses the absorber and the thermal insulation of the collector, protecting them from moisture and mechanical damage.

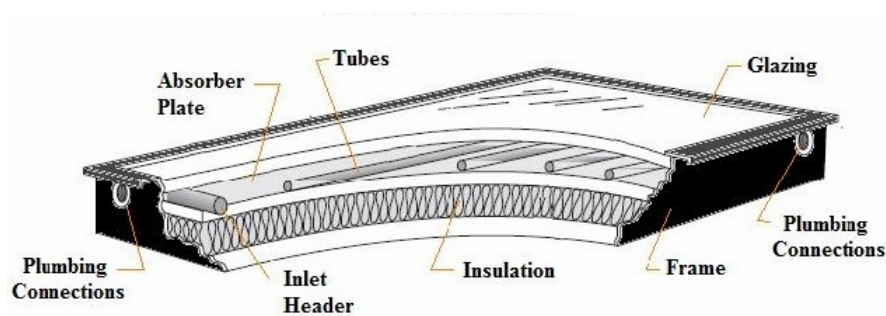


Figure 1.25: Flat plate collector [15]

1.9.4 How does a flat plate collector work

Part of the solar radiation that reaches the glass pane passes through it to reach the absorber plate. This plate heats up and transfers the heat to the heat transfer fluid which circulates in the tubes. Like any body that heats up, the absorber emits radiation (mainly in the infrared range) which is reflected by the glass, this is the principle of the "greenhouse effect". The function of the insulator is to minimise heat loss to the outside. Indeed, most of the energy absorbed must be transmitted to the fluid, so losses to the surrounding environment must be minimised.

ADVANTAGES:

- Economic price

- Reliability
- Long service life
- Energy efficiency
- Integration into roofs

Disadvantages:

- Not suitable for high temperatures
- The internal temperature can rise very high when there is no liquid circulation.

1.9.5 Parameters characterising the operation of a flat plate collector

These parameters can be classified into two categories: external and internal parameters.

External parameters

The main external parameters that can directly influence the performance of a flat plate collector are:

- solar radiation, position of the sun, duration of insolation, ...etc
- Ambient temperature
- Wind speed

Internal parameters**Geometric parameters:**

- Positional parameters: tilt angle, orientation of the collector.
- The surface of the collector
- Dimensions of different elements: thickness, length and width

Working parameters:

- The inlet temperature of the heat transfer fluid.

- The mass flow rate of the heat transfer fluid.
- The temperatures of the different elements of the collector

These parameters are very important. They allow, taking into account the cost, to have a high fluid outlet temperature (high power output). In other words, a better efficiency of the collector.

1.10 Applications of flat plate solar collectors

Flat-plate thermal collectors are integrated in several solar heating techniques. These include

1.10.1 Domestic water heating

Domestic hot water heating is one of the most accessible solar technologies for individuals. The principle is simple: flat-plate thermal collectors convert light radiation into heat. The heat transfer fluid circulates in the thermal collectors and transports the heat to the domestic water stored in a tank. Of course, there are several systems for heating domestic hot water, each with its own advantages and disadvantages [16].

1.10.2 Room heating

Room heating from flat plate solar collectors is not yet very developed, although developed, although the evolution of building insulation standards may make this technology more attractive. The main obstacle is that the need for heating is mainly in winter, when there is less sunlight [16].

There are three ways to heat a room with solar thermal energy: with conventional radiators, with warm air ventilation or with underfloor heating.

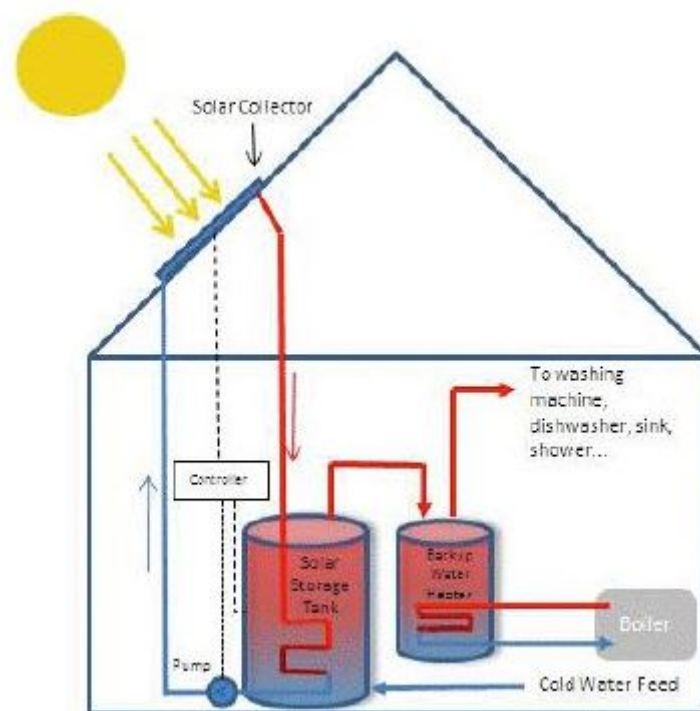


Figure 1.26: Conventional solar water heating system [2]

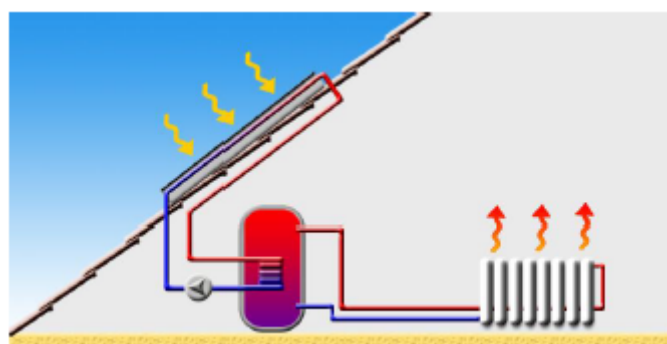


Figure 1.27: Room heating system [16]

1.10.3 Indirect drying of agricultural products

Natural drying of agricultural products is a traditional method of solar drying that uses the action of solar radiation and convective movements of the ambient air to reduce the moisture content of the product to be dried in order to preserve it better. During the natural drying process, the products are generally not protected from the weather or from insects. This results in their progressive soiling, exposure to micro-organisms and thus infection. In order to obtain better quality dried products, to accelerate the drying process and to reduce its strong dependence on climatic conditions, the use of artificial dryers with flat solar collectors (indirect drying) can

be considered as the best way to overcome the problems encountered during the direct drying process [16].

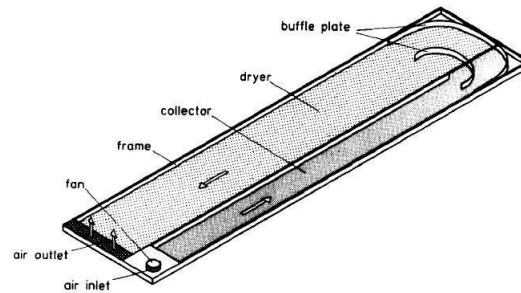


Figure 1.28: Utilization of Solar Air Collectors for Product's Drying Processes [17]

The operating principle of an indirect solar thermal dryer is based on the heating of the products to be dried by the hot air coming out of the flat solar collector. This heating, under controlled conditions, causes a decrease in the relative humidity and reduces the drying time.

Chapter 2

mathematical modeling

2.1 Introduction

To solve a fluid mechanics or heat transfer problem, it is possible to solve it either mathematically (analytical solution) or numerically (numerical solution). The analytical solutions, based on the local form of the problem (Partial Differential Equations: "PDE" associated with initial and boundary conditions), cannot be determined in the case. The problem under study (the flow and heat exchange inside a flat plate solar collector) is modeled by the partial differential equations of conservation of mass, momentum and energy. These equations are known as the Navier-Stokes equations. These equations are strongly coupled to each other and they are not linear. In general, these equations do not admit analytical solutions except in very simplified cases [30]. The general analytical solution of these equations fits into in the seven millennium problems. The objective of this chapter is therefore to present the mathematical model governing the problem studied. First, the geometry of the sensor studied will be presented. Then, the mathematical formulation of the Navier-Stokes equations will be presented for the two flow regimes: laminar and turbulent.

2.2 Setting up the problem into equations :

The advantage of writing the differential equations describing the turbulent flow in general form is to construct a general numerical procedure that applies for the different equations considering the specific boundary conditions. It is known that for some cases of simple flows an exact analytical solution is possible. For the general case of turbulent flows, the system of Navier-Stokes equations cannot be solved directly due to the non-linearity of the equations and the appearance of the Reynolds constraints of the turbulence as new unknowns in the transport equations. The system of equations is closed using turbulence models. In fluid mechanics, the fluid is assumed to be a continuous, which allows the use of the classic conservation laws, which are [18][19]: 1. Conservation of mass. 2. Conservation of momentum. 3. Conservation of energy.

The mathematical formulation of conservation laws governing physical phenomena, such as fluid flows, is usually written in the form of partial differential equations as follows:

2.2.1 Continuity equation :

The differential equation describing the principle of conservation of mass and is expressed mathematically, for the case of a stationary flow, as :

$$\frac{\partial}{\partial t}\rho + \frac{\partial}{\partial x}(\rho.u) + \frac{\partial}{\partial y}(\rho.v) + \frac{\partial}{\partial z}(\rho.w) = 0 \quad (1)$$

Where t is time, u , v and w are the components of the fluid velocity in the x , y and z directions respectively.

or in a more compact notation, we have :

$$\frac{\partial}{\partial t}\rho + \text{div}(\rho u) = 0 \quad (2)$$

for an incompressible fluid we have : $\partial u \frac{\partial v}{\partial x} + \frac{\partial w}{\partial y} = 0$

Physically, it represents the change in properties with time following a given element of mass as it moves through the fluid.

2.2.2 Momentum equation :

The principle of conservation of momentum establishes the relationships between the characteristics of the fluid as it moves and the causes that produce it. It states that the rate of change of momentum contained in the control volume is equal to the sum of all external forces applied to it. The momentum equations (or Navier-Stokes equations) for incompressible Newtonian fluids in the laminar regime are given by the following expressions : following x :

$$u \frac{\partial u}{\partial x} + v \frac{\partial u}{\partial y} + w \frac{\partial u}{\partial z} = -\frac{1}{\rho} \frac{\partial P}{\partial x} + \mu \left(\frac{\partial^2 u}{\partial x^2} + \frac{\partial^2 u}{\partial y^2} + \frac{\partial^2 u}{\partial z^2} \right) \quad (3)$$

following y :

$$u \frac{\partial v}{\partial x} + v \frac{\partial v}{\partial y} + w \frac{\partial v}{\partial z} = -\frac{1}{\rho} \frac{\partial P}{\partial y} + \mu \left(\frac{\partial^2 v}{\partial x^2} + \frac{\partial^2 v}{\partial y^2} + \frac{\partial^2 v}{\partial z^2} \right) \quad (4)$$

following z :

$$u \frac{\partial w}{\partial x} + v \frac{\partial w}{\partial y} + w \frac{\partial w}{\partial z} = -\frac{1}{\rho} \frac{\partial P}{\partial z} + \mu \left(\frac{\partial^2 w}{\partial x^2} + \frac{\partial^2 w}{\partial y^2} + \frac{\partial^2 w}{\partial z^2} \right) \quad (5)$$

2.2.3 Energy equation :

It is derived from the law of conservation of energy. It is written as follows:

$$\left(\frac{\partial (\rho u T)}{\partial x} + \frac{\partial (\rho v T)}{\partial y} + \frac{\partial (\rho w T)}{\partial z} \right) = \frac{\partial}{\partial x} \left[\left(\frac{\mu}{Pr} \right) \frac{\partial T}{\partial x} \right] + \frac{\partial}{\partial y} \left[\left(\frac{\mu}{Pr} \right) \frac{\partial T}{\partial y} \right] + \frac{\partial}{\partial z} \left[\left(\frac{\mu}{Pr} \right) \frac{\partial T}{\partial z} \right] \quad (6)$$

Where: u , v and w represent the velocities of the flow in the x , y and z directions respectively. P is the pressure. T , is the temperature. μ , is the dynamic viscosity of the fluid. $Pr = \frac{c_p \rho \mu}{\lambda}$, represents the Prandtl number.

The set of all equations (1 to 6) forms the Navier-Stokes equations for a Newtonian, stationary, three-dimensional, viscous (non-perfect) fluid.

2.2.4 Flow regimes : Laminar and turbulent

A flow is laminar when the movement of the fluid particles is regular and orderly. Flow is turbulent when the motion is irregular and random fluctuations in velocity are superposed on the mean motion of the fluid. One of the first analyses of the transition from a laminar regime to turbulence, based on observations of flows in a cylindrical duct, was performed by Reynolds in 1883 [31]. Reynolds showed that the transition from the laminar to the turbulent regime does not depend separately on each parameter but on a single quantity grouping them all together. For a viscous fluid of density ρ and dynamic viscosity μ , passing through a pipe of diameter D with an average velocity U , the Reynolds number (Re) is defined as: $Re = \frac{\rho U D}{\mu}$ [18] [32].

The Reynolds number is a dimensionless quantity representing the ratio of inertial forces to viscosity forces, and characterises the occurrence of turbulence [32].

Experience shows that for internal flows (flows in pipes), the critical Reynolds number (Re_{cr}) for switching from laminar to turbulent is approximately equal to $Re_{cr} = 2300$.

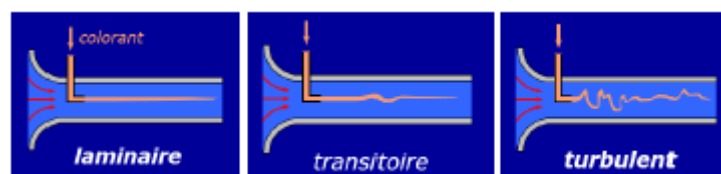


Figure 2.1: the transition from the laminair to the turbulent regime: the reynolds experience [18]

Description of turbulence :

Most flows found in the real world are turbulent, the term actually denoting a motion in which an irregular fluctuation is superimposed on the main flow. the main flow. Turbulence is governed by the Navier-Stokes equations, as it is characterised by spatial and temporal scales of very different sizes. According to Reynolds [31] turbulence is defined by the irregular and random motion in space and time, which appears significantly in flows with high Reynolds numbers.

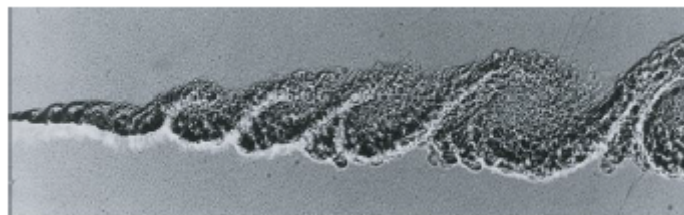


Figure 2.2: visualisation of a turbulent flow [19]

2.3 Principle of the finite volume method:

The finite volume method was first described in 1971 by Patankar and Spalding and published in 1980 by Patankar (Numerical Heat Transfer and Fluid Flow). It is a discretization technique that converts conservation partial differential equations into algebraic equations that can be solved numerically. In this method the domain is divided into a finite number of control volumes that cover the computational domain. The control volume technique consists of the integration of the partial differential equations over each control volume to obtain discretised equations that preserve all physical quantities over a control volume. On each control volume or cell the conservation laws are applied to determine the different variables associated with the problem at points (or nodes) that do not necessarily correspond with the points of the mesh or grid. The mesh associated with the calculation can be structured or unstructured as for example in finite elements, which gives a great flexibility to the method.

advantages: - Preservation of the conservative character of the equations on each control volume (continuity of the flows at the interfaces), valid for any fineness of the mesh - Relatively easy to implement; - Applicable to complex geometries; - Reasonable computation time and memory storage (sparse matrix).

Disadvantages: - Less accurate than spectral methods.

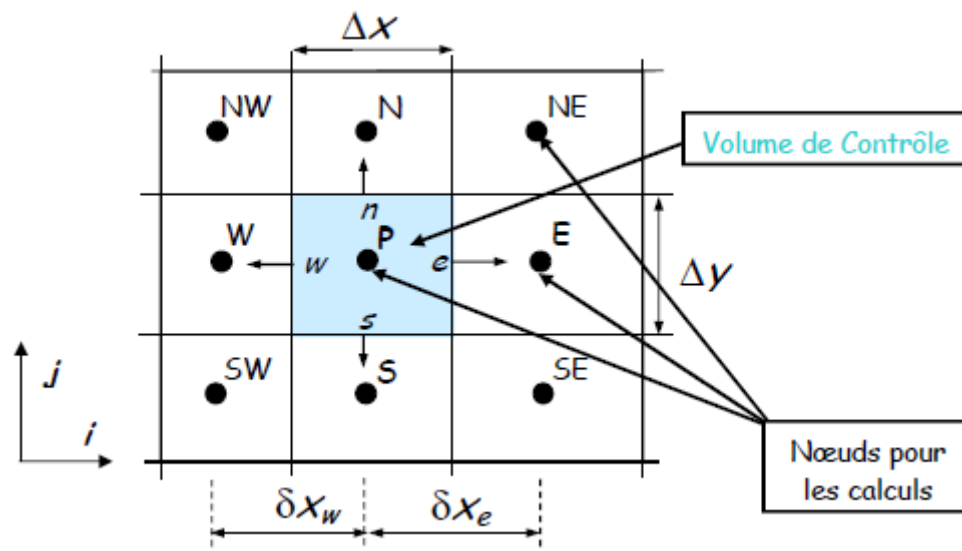


Figure 2.3: structured mesh

2.3.1 Description of a control volume

In finite volume simulation, the computational domain is divided into a finite number of elementary subdomains, called control volumes. The finite volume method consists of integrating the partial differential equations over each control volume. Each of these (control volume) contains a node called the node. An example of a control volume is shown in (fig 2.4). For a main node (P'), the points E and W (E : East, W : West) are neighbours in the X direction, while N and S (N : North, S : South) are neighbours in the Y direction. The surrounding control volume (P') is shown by the dashed lines. The faces of the control volume are located at points (e) and (w) in the X direction, (n) and (s) in the Y direction [33].

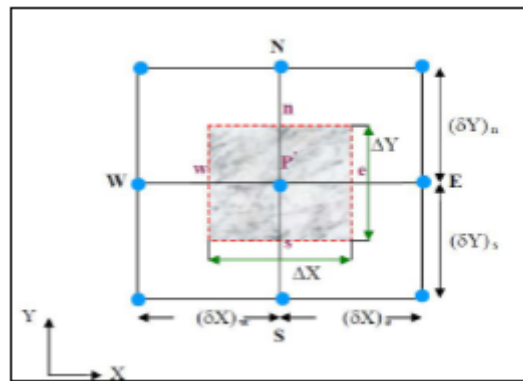


Figure 2.4: schematic representing a two-dimensional control volume

2.4 Subdivision of the study domain (mesh)

The location of the variables of the problem to be computed is defined by the mesh (or grid) which corresponds to a discrete representation of the physical domain to be represented. The computational domain is then divided into a finite number of elements and control volumes that do not necessarily coincide (as we will see later). The distinction we make here between elements and control volumes is essential. We call here an element a surface or a 3D volume created from points and which is only used in the construction of the mesh and allows the spatial discretisation of the medium. The control volume corresponds to a surface or a volume in which the balance equations are calculated. The discretization of the domain is obtained by a mesh consisting of a network of points (nodes).

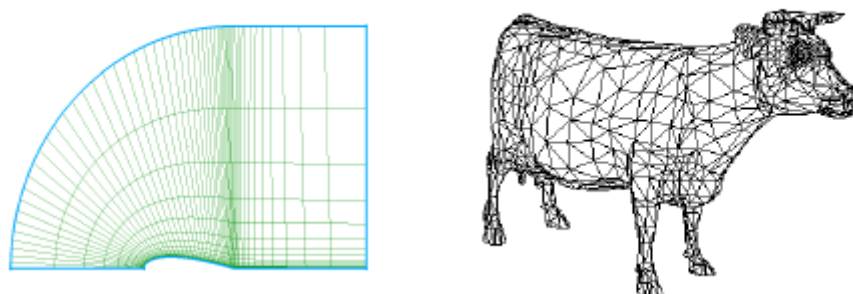


Figure 2.5: Examples of the structured (left) and unstructured mesh (right)

The possibilities offered by the finite volume method are very varied and We present here only an overview of the most commonly used meshing techniques:

2.4.1 STRUCTURED MESHES

In this category the possibilities are numerous, the calculation grid can be regular, or structured by blocks, with or without overlapping subdomains. The calculation grid can be regular, or structured by blocks, with or without overlapping subdomains. In general, the implementation of the finite volume method is easier in this category, it often leads to simpler numerical schemes and in particular to "band" structures of the matrix systems to be solved when using an implicit scheme for example. The associated data structure is simplified compared to a non-structural finite element mesh and the method is more efficient in terms of computation time. However, complex domains are difficult to represent.

CARTESIAN STRUCTURAL GRIDS

In this category we find the purely cartesian grids, i.e. the dimensions of the elements are parallel to the axes of a cartesian reference frame and which can therefore be created very easily. It can be regular (Figure 2.6), i.e. that two neighbouring points are always at the same distance, or irregular if this is not the case. or irregular if this is not the case.

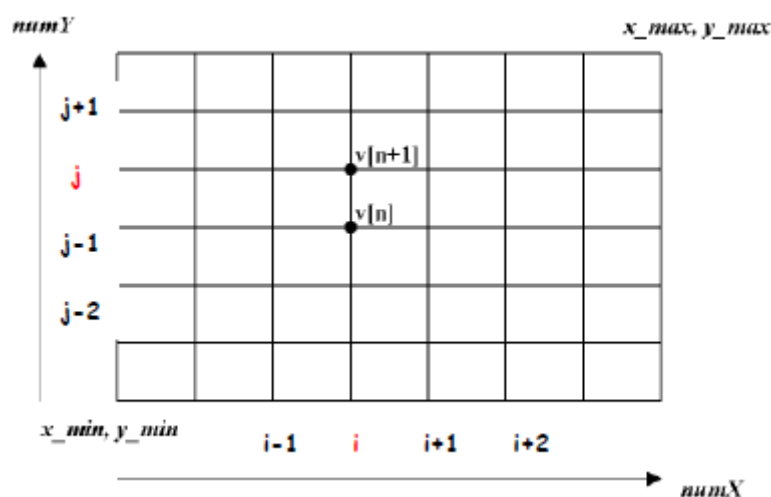


Figure 2.6: regular cartesian grid

The positions of the grid points are then simply marked by a set of two or three

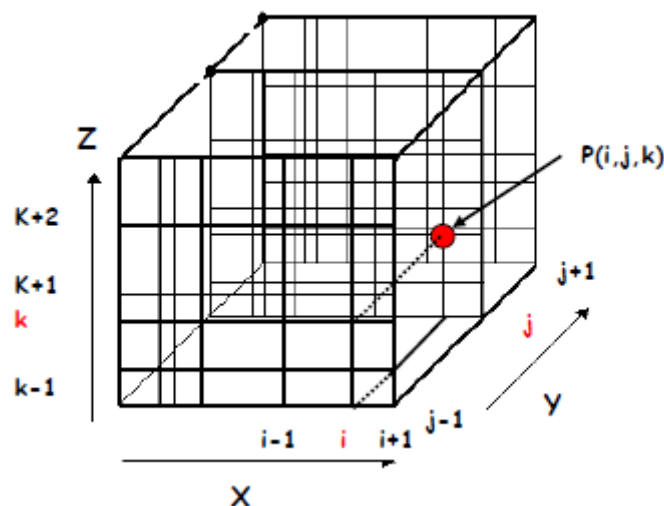


Figure 2.7: irregular cartesian grid

indices i, j, k . Each grid point thus has 4 "close" neighbours in 2D and 6 for a three-dimensional mesh. This makes it very easy to identify the neighbours of a grid node, which greatly simplifies the programming of the method and allows us to obtain matrices whose regular structure can be exploited for an efficient resolution with an implicit scheme.

CURVILINEAR STRUCTURAL GRIDS (BODY FITTING)

This technique allows better representation of boundary conditions for more complex geometries. It requires a transformation from the physical to the computational domain. The equations to be solved are then more complex, which makes the calculations more complex and requires precautions if we want to keep the conservative character of the numerical schemes used and keep a good accuracy. In general, this method is rarely used with finite volumes, but is used to construct the mesh, the equations being solved directly on the physical domain.

BLOCK STRUCTURED GRIDS

When using a structural mesh it is very difficult to represent complex geometries, especially in 3D. To represent more "industrial" geometries and for example to refine some parts of the mesh, a block structure mesh can be used. Cartesian or

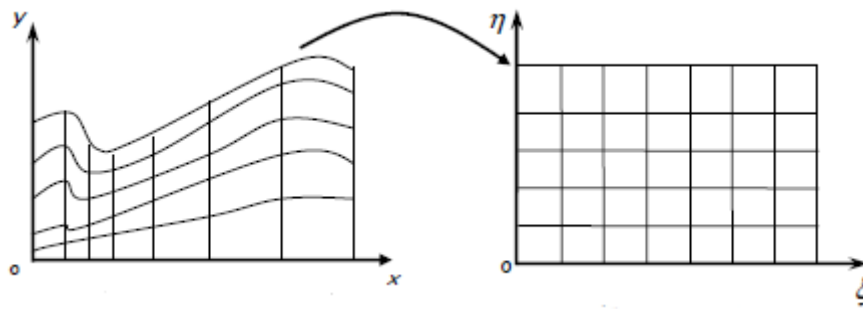


Figure 2.8: Transformation from physical domain to computational domain

non-orthogonal grids can be used. In the case where there is perfect coincidence between the different blocks, the method is then particularly efficient on parallel machines or in the calculations, each block can be attributed to a processor.

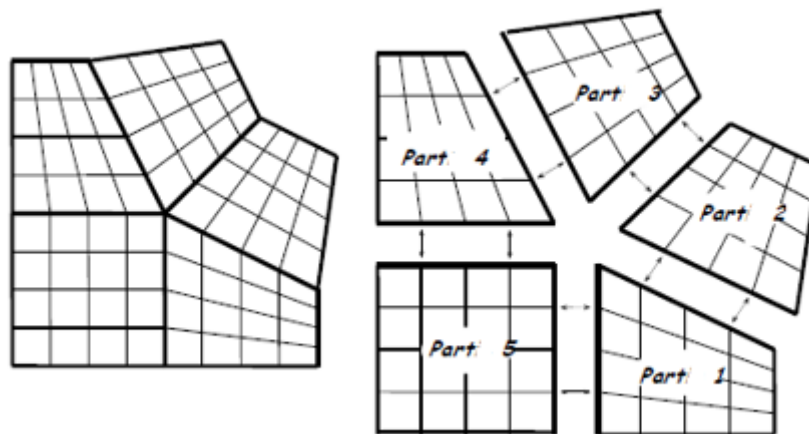


Figure 2.9: BLOCK STRUCTURED GRID

It is not necessary, however, that there be a perfect match at the interface of each block. This is referred to as non-conforming grids or grids with non-conforming interfaces. In this case we add some complexity to the solver because a particular treatment of the interfaces is necessary to calculate the flows. On the other hand, it is possible to build the different domains separately and use finer meshes in certain regions (or blocks) or to "glue" two different meshes. Again this method offers interesting possibilities for implementation on parallel machines using the sub-domain method.

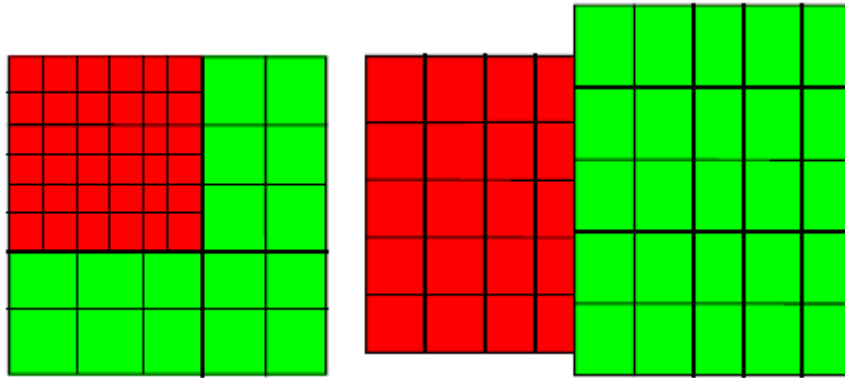


Figure 2.10: refined mesh (left) and different mesh (right)

Composite mesh (Chimera grid)

In this method, several blocks are used to represent the domain, for which there is an overlap of grids. In regions where there is overlap of several grids, the boundary conditions between the domains are obtained by interpolating the solutions of the different domains. This method makes it easier to deal with very complex geometries while using a structural mesh. This method is used, among other things, to track the motion of solid bodies. In this case a block is attached to the moving body and moves with it while a fixed grid covers the rest of the domain.

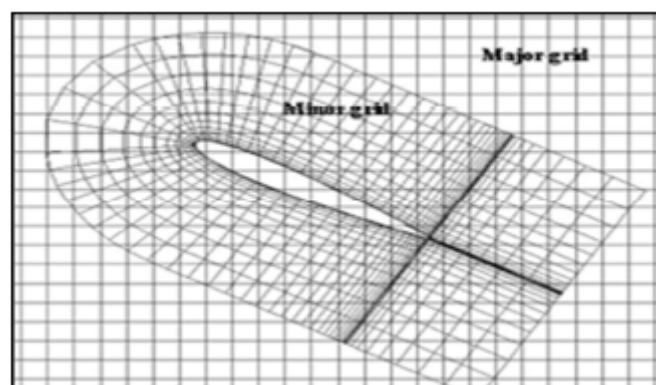


Figure 2.11: chimera grid

The advantage of this method is the possibility of creating meshes that are completely independent of each other, without any coincidence between the interfaces of the different domains. The major difficulty that arises is related to the flow conservation properties that are difficult to obtain and implement at the

interfaces of the different domains.

2.4.2 UNSTRUCTURED MESHES

This category of meshes offers the greatest flexibility in the construction of complex geometries. Indeed it is always possible to create meshes (or grids) automatically with 2D triangles (and 3D tetrahedrons), regardless of the complexity of Whatever the complexity of the domain envelope. In practice we prefer to use quadrangles and hexaedra which allow to obtain a better precision in calculations.

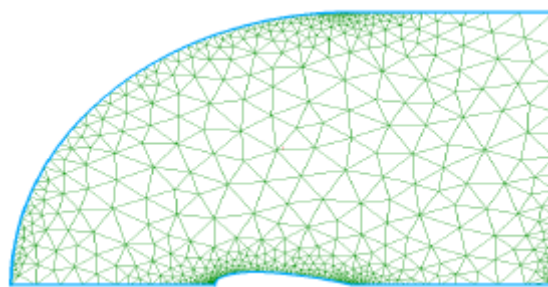


Figure 2.12: unstructured triangle mesh

The construction of unstructured meshes is in general much simpler and faster to implement in an industrial calculation context. It is also easier to refine locally some part of the domain.

Another advantage of unstructured meshes is that the nodes and connectivity do not have a global structure like structural meshes. Thus it is possible to add or remove nodes and/or elements during the calculation if needed.

2.4.3 MIXED MESHES

As the name implies, mixed meshes are composed of structural meshes in certain regions and non-structural meshes when the geometry is more complex. The meshes are usually connected "node to node" but can also have non-conforming interfaces.

This method improves the performance of the calculations compared to a unstructured mesh.

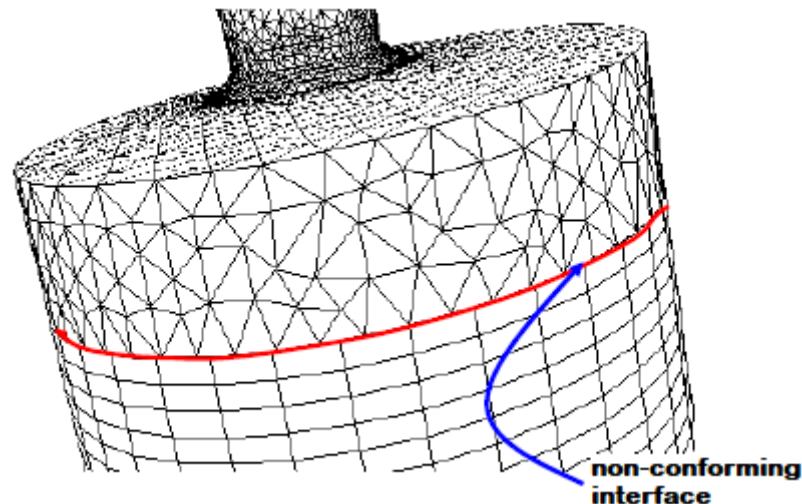


Figure 2.13: mixed mesh with non-conforming interface

2.4.4 General mesh generation techniques

In practice, there is no precise rule for creating a valid mesh, but there are different approaches to obtaining an acceptable grid. We can summarise these rules as follows:

- Maintain good feature quality.
- Ensure good resolution in high gradient regions.
- Ensure good smoothness in the transition areas between the fine and coarse mesh parts.
- Ensure good smoothness in the transition areas between fine and coarse mesh parts.
- Minimise the total number of elements (reasonable calculation time).

2.4.5 Mesh quality

The generation of a very good mesh quality is essential for an accurate, robust and meaningful calculation result. Good mesh quality is based on the following elements

- Minimisation of skewness elements;
 - Good resolution in regions with a strong gradient (boundary layers, shock waves, etc.)
- Finally, the quality of the mesh has a serious impact on the convergence, the accuracy of the solution and, above all, the computation time. solution and especially the computation time.

2.5 Discretisation by the finite volume method

The discretization of the domain is obtained by a mesh consisting of a network of points (nodes). Thus a volume element (control volume) is defined around each node. After selecting the differential equations to be solved, it is necessary to transform these differential equations into algebraic equations where the continuous variations of the flow variables are represented by values at discrete points in time and space. The discrete locations in space are represented by nodal points (or nodes) chosen in a numerical grid that subdivides the flow domain according to the nature and geometry of the computational domain.

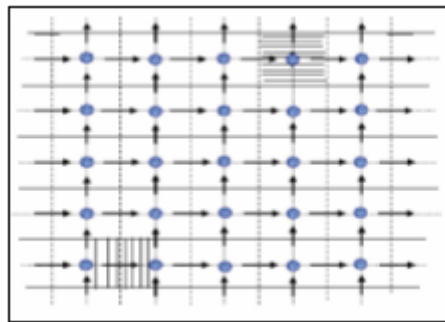


Figure 2.14: the principle of staggered meshing

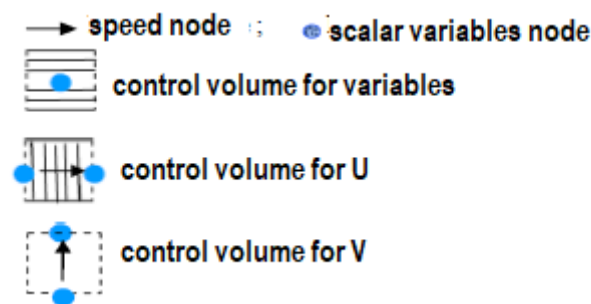


Figure 2.15: staggering meshing figure's symbols definition

2.5.1 Discrete equations

The mathematical equations outlined above governing flow express the transport of mass, momentum and energy quantities. The transport differential equations can be converted into a system of algebraic equations the into one equation. This equation is

written in the stationary, two-dimensional case as follows [34, 35] :

$$\frac{\partial}{\partial x} (\rho U \phi) + \frac{\partial}{\partial y} (\rho V \phi) = \frac{\partial}{\partial x} \left(\Gamma \frac{\partial \phi}{\partial x} \right) + \frac{\partial}{\partial y} \left(\Gamma \frac{\partial \phi}{\partial y} \right) + S \phi \quad (7)$$

To understand this method, we consider the simplest case. Let us consider the one-dimensional steady flow in which only the convection and diffusion terms are present. The governing differential equation in this case is :

$$\frac{d}{dx} (\rho u \phi) = \frac{d}{dx} \left(\Gamma \frac{d\phi}{dx} \right) \quad (8)$$

The continuity equation is written :

$$\frac{d}{dx} (\rho u) = 0 \quad ; \text{where } \rho u = \text{constant} \quad (9)$$

To obtain the discretized equation, the three-node system, shown in Figure III-3, is used. It is assumed that "e" is located in the middle between P and E, and w is between W and P.

the integration gives us :

$$(\rho u \phi)_e - (\rho u \phi)_w = \left(\Gamma \frac{d\phi}{dx} \right)_e - \left(\Gamma \frac{d\phi}{dx} \right)_w \quad (10)$$

$$(\rho u)_e - (\rho u)_w = 0 \quad (11)$$

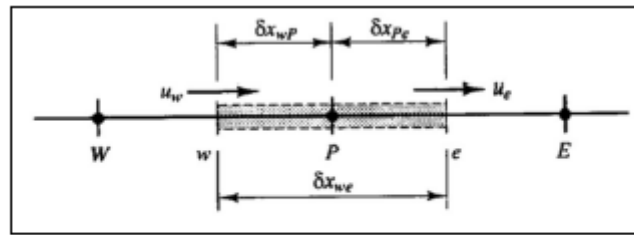


Figure III-3: Volume de contrôle autour du nœud P, cas monodimensionnel.

Figure 2.16: control volume around the node p (one-dimensional case)

2.6 Conclusion

This chapter was reserved for the mathematical modelling of our study. The classic conservation equations and the finite volume method, a mathematical discretization technique to transform the differential writing of the governing equations into an algebraic writing, were briefly presented. - The visible non-linearities in the equations are mainly responsible for the difficulties in obtaining an analytical solution. Therefore, the use of numerical methods is essential to work on this simulation. The Gambit and Fluent software based on the finite volume method were used to solve the different equations (chapter 3). The methodology and the logic of the solution followed have been explained. The physical parameters, geometry, initial and boundary conditions applied were defined. The results of the numerical simulations are presented in the last chapter. As it is necessary to explain the way the numerical simulation is developed on the CFD software FLUENT, the following chapter is reserved for the presentation of this calculation code. This chapter ends with the discretized equations and a conclusion.

Chapter 3

Problem's position

3.1 Introduction

Numerical modelling and simulation is an important conception tool used to predict experimental implementation. In any solar energy application, it would be advisable to analyse theoretically any given system in as much detail as possible before moving on to the experimental stage.

Numerical simulation is almost always in the form of a computer program or tools known as simulation environments capable of transforming differential equations into algebraic equations in which continuous variations of flow variables are represented by values at discrete points in time and space.

Simulation does not replace, but rather enhances, experimentation. It allows the analysis of the problem to be performed under realistic conditions (reproducing experimental tests to better understand them and at a lower cost) or, on the opposite, under extreme/marginal test conditions (extreme climates, installation flaws). These latter cannot be done by experimentation (due to costs...), so simulation expands the field of tests for a system.

Through simulation, the system under study becomes more flexible. Parametric studies can easily be done. The use of simulation can also vary the time scale for a

study, which is otherwise impossible.

The studied model is based on the conservation of mass and momentum equations (Navier Stokes), which are coupled with the conservation of energy equation, discretised by the finite volume method, governing the laminar airflow inside a rectangular shaped canal.

In this work, the creation of the geometrical model, the mesh, the definition of the boundaries were generated with the help of ANSYS-Gambit 2.4.6 software, which is a computer design software. To determine the evolution of the (X, Y, Z)-temperature profiles of the air inside a rectangular canal and the absorbing wall of a planar air collector, we chose the commercial code ANSYS-FLUENT 14.5 which allows the simulation of different types of flows with complex geometries. It can solve the equations governing laminar and turbulent, stationary and unsteady fluid motion. It can solve flow problems with structured and unstructured meshes, regardless of the complexity of the geometry, with relative ease. The meshes supported in 2D are triangular or quadrilateral, in 3D they are tetrahedral, hexahedral or pyramidal, or mixed (hybrid) meshes.

FLUENT facilitates the user's manipulation through the simplicity of its graphic interface. The code is not limited only by its own functions, but it offers the user the possibility to inject his own function and define any particularities of his problem.

3.2 Physical model

In this work, we will choose to study a flat plate air collector intended in our case for a solar dryer (see figure 00). A flat plate air collector is generally composed of a box, a glazing, an insulation, an absorber and a canal allowing the passage of air.

The geometry of the proposed system is shown in the following figures (quote figures...?). It is a flat plate air collector made up of three main parts: a part for the confined air located at the top of the collector, a part for the thermal insulation located at the bottom of the collector, and a part located in the centre of the collector,

between the top part and the lower part, intended for the canal in which the air to be heated circulates. The passage of the air through the canal allows it to gain heat through convective heat exchange with the absorber plate before it reaches the outlet. A small amount of the incident solar radiation is absorbed by the glass cover. The rest is reflected back into the upper part of the solar collector and transmitted through the confined air to the absorber, which absorbs the large amount of energy. The enclosed air technique provides us with an additional heat source through the greenhouse effect in the upper part of the collector. The dimensions of the physical

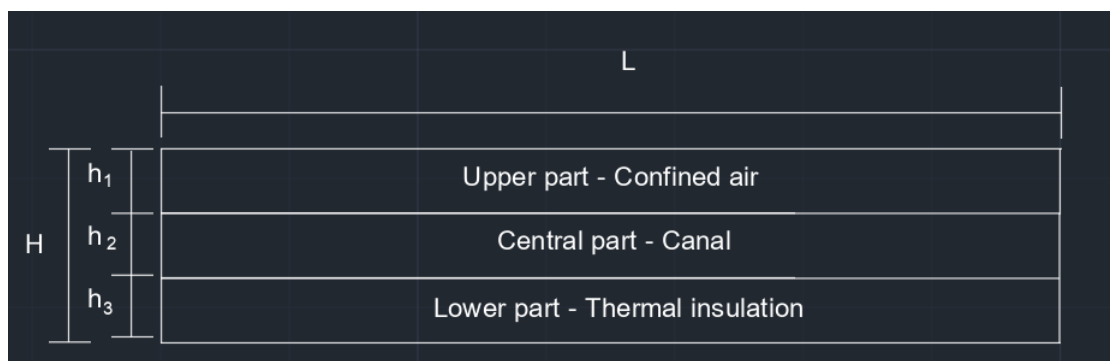


Figure 3.1: cross section of the collector with dimensions

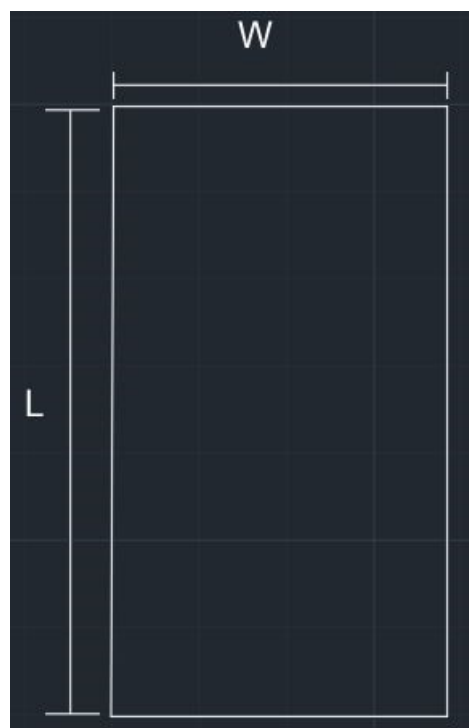


Figure 3.2: a view from above on the collector dimensions

model are shown in Figures 4.1 and 4.2. It is a rectangular flat plate air collector with

length of L , width of W and height of H . The height of the solar collector consists of three parts: a part at the top of the collector of height h_1 , a part in the centre of the collector of height h_2 , and a part at the bottom of the collector of h_3 . The geometric and physical parameters are given in two following Tables

Tables of physical parameters

Size	Symbol	Unit
Length of the box	L	cm
Height of the main enclosure	H	cm
Width of the box	W	cm
Height of the confined air part	h_1	cm
Height of the canal part	h_2	cm
Height of a part of the main enclosure tubes	h_3	cm

Table 3.1: symbols and units for collector dimensions

Collector's dimension	value
L	94
H	6
W	36
h_1	2
h_2	2
h_3	2

Table 3.2: collector's dimensions

Materials	Thermal Conductivity (W/m K)	Density (Kg/m ³)	Specific Heat « C_p » (J/kg K)
Copper	387.6	8978	381
Wood	0.173	700	2310
Glass	1	250	720

Table 3.3: Physical properties of materials used in the simulation

3.3 Mathematical formulation

3.3.1 Simplifying assumptions

In order to solve the equations governing the three-dimensional flow of air through the canal of a flat plate air collector, the following simplifying assumptions will be adapted:

- The three-dimensional flow assumed to be stationary in the laminar regime.
- The three-dimensional flow of air presented as a Newtonian fluid, with constant properties.
- The cover is opaque to IR radiation and does not absorb solar radiation.

The equations describing the airflow phenomenon inside the solar collector are the following:

Continuity equation :

$$\frac{\partial u}{\partial x} + \frac{\partial v}{\partial y} + \frac{\partial w}{\partial z} = 0 \quad (1)$$

Momentum equation :

following x :

$$u \frac{\partial u}{\partial x} + v \frac{\partial u}{\partial y} + w \frac{\partial u}{\partial z} = -\frac{1}{\rho} \frac{\partial P}{\partial x} + \mu \left(\frac{\partial^2 u}{\partial x^2} + \frac{\partial^2 u}{\partial y^2} + \frac{\partial^2 u}{\partial z^2} \right) \quad (2)$$

following y :

$$u \frac{\partial v}{\partial x} + v \frac{\partial v}{\partial y} + w \frac{\partial v}{\partial z} = -\frac{1}{\rho} \frac{\partial P}{\partial y} + \mu \left(\frac{\partial^2 v}{\partial x^2} + \frac{\partial^2 v}{\partial y^2} + \frac{\partial^2 v}{\partial z^2} \right) \quad (3)$$

following z :

$$u \frac{\partial w}{\partial x} + v \frac{\partial w}{\partial y} + w \frac{\partial w}{\partial z} = -\frac{1}{\rho} \frac{\partial P}{\partial z} + \mu \left(\frac{\partial^2 w}{\partial x^2} + \frac{\partial^2 w}{\partial y^2} + \frac{\partial^2 w}{\partial z^2} \right) \quad (4)$$

Energy equation :

$$\left(\frac{\partial(\rho u T)}{\partial x} + \frac{\partial(\rho v T)}{\partial y} + \frac{\partial(\rho w T)}{\partial z} \right) = \frac{\partial}{\partial x} \left[\left(\frac{\mu}{Pr} \right) \frac{\partial T}{\partial x} \right] + \frac{\partial}{\partial y} \left[\left(\frac{\mu}{Pr} \right) \frac{\partial T}{\partial y} \right] + \frac{\partial}{\partial z} \left[\left(\frac{\mu}{Pr} \right) \frac{\partial T}{\partial z} \right] \quad (5)$$

3.3.2 Steps involved in creating the sensor geometry :

The solver's choice :

The numerical calculation will be performed using FLUENT 14.5. For this purpose, the type of solver (FLUENT 5/6) was chosen in GAMBIT

Creation of the geometry

The geometry of the system has been created using the predefined geometries since our model is made in 3D.

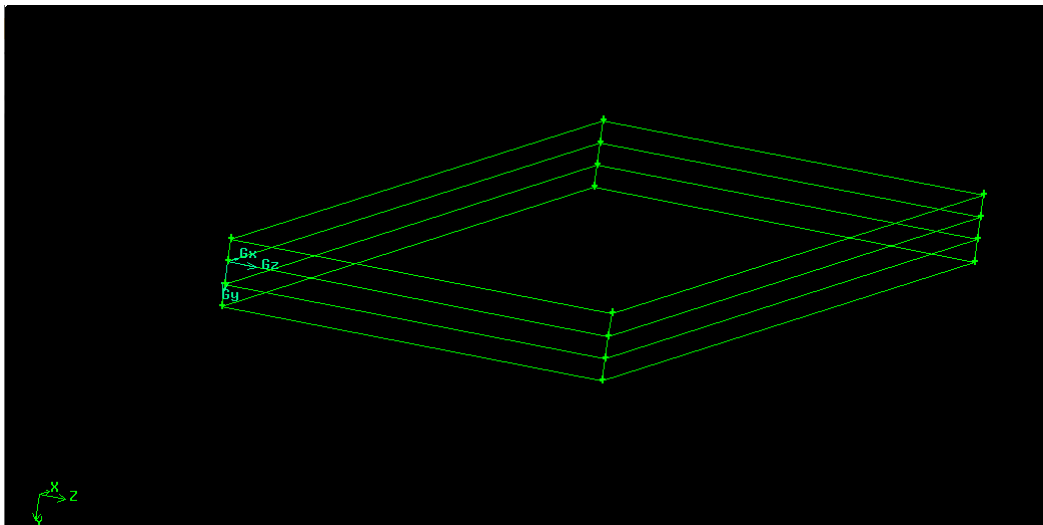


Figure 3.3: suggested collector design using Gambit

3.4 Mesh

To generate a mesh, the following steps are required:

- Creating the geometry of the physical model.
- choosing a suitable mesh for the physical model.

- defining the parameters of the calculation zones.

A hexahedral mesh was adopted for the numerical simulation because the proposed system is geometrically simple and does not require complex shapes. The mesh used corresponds to a total number of 84780 cells, and seems to give the best precision-speed of convergence ratio.

- We start the mesh by choosing « MESH COMMAND BUTTON »



Figure 3.4: mesh commande button

- We click on « VOLUME COMMAND BUTTON »

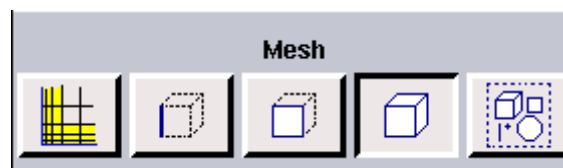


Figure 3.5: volume commande button

Then click on "MESH VOLUMES" and choose 0.8 for "Spacing" and "hexahedral" as elements.

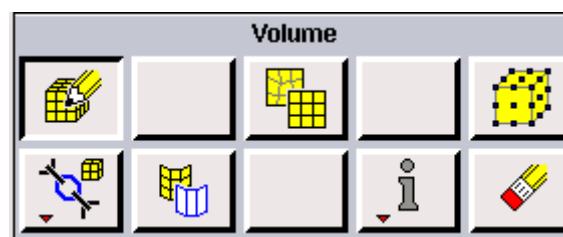


Figure 3.6: mesh commande button

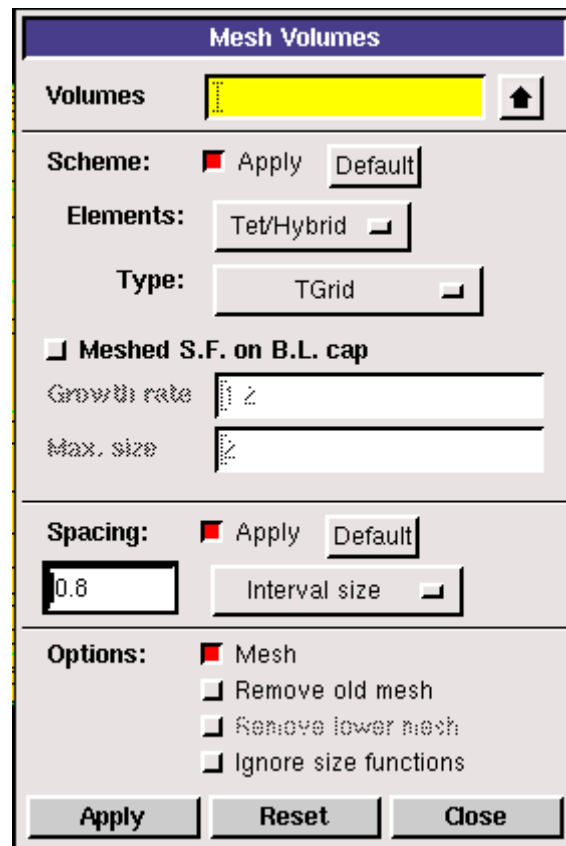


Figure 3.7: definition of the mesh parametrs

The generation of the hexahedral mesh is presented in the figures 4.8 and 4.9 :

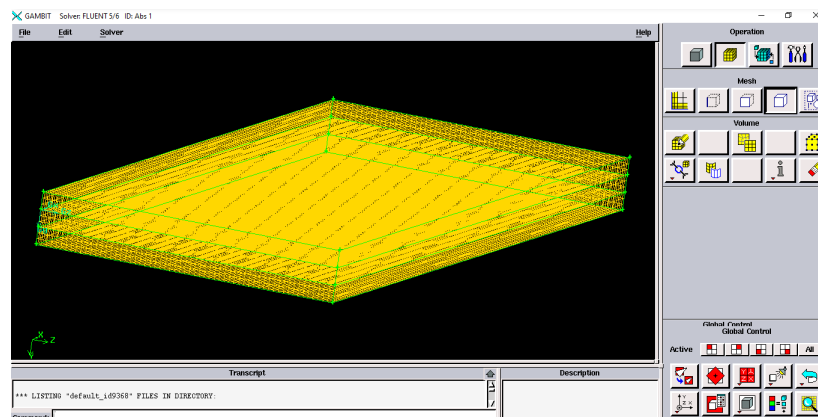


Figure 3.8: a view of the collector's hexahedral mesh

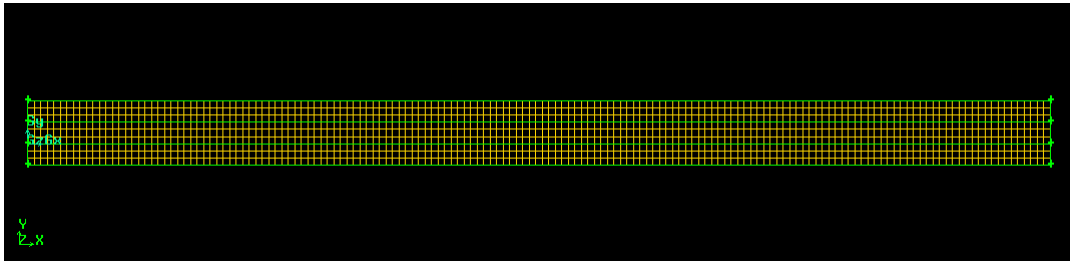


Figure 3.9: side view of the collector's hexahedral mesh

3.5 Boundary conditions

- The solution of the momentum equation as well as the energy equation requires the definition of initial conditions and boundary conditions on the boundaries of the computational area. The different conditions applied in our study are illustrated in the figure 4.10 :

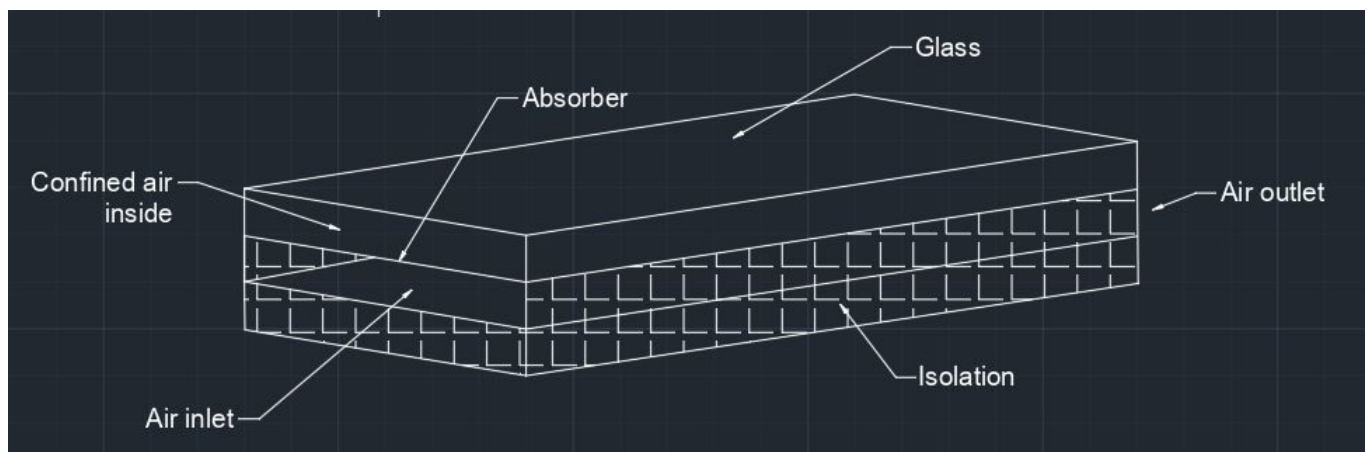


Figure 3.10: boundary conditions definition

3.5.1 Initial conditions

-Velocities and daytime temperatures :

Velocity 1	Velocity 2	Velocity 3	Velocity 4
0.1 m/s	0.3 m/s	0.08 m/s	0.05 m/s

Table 3.4: suggested velocities

The different temperatures obtained using the URER-MS daily archive for the day of

January 5, 2020 in the Adrar region are shown in Table 4.5.

Time of the day	Temperature (K)	Direct solar irradiation (w /m ²)	Diffuse solar irradiation (w /m ²)
8:00	274.75	189	7
10:00	278.95	922	49
12:00	285.95	1025	60
13:30	289.95	1044	60
14:00	291.05	1037	60
16:15	293.15	903	55
20:00	286.75	0	0

Table 3.5: different parameters of the 5th of January 2020 obtained from the URER-MS daily archive.

- The ANSYS-GAMBIT software allows to define the different regions of the physical model as well as the different boundary conditions.

3.5.2 Definition of the regions

The flat plate air collector consists of three regions:

- The upper region (for the confined air)
- The lower region (for thermal insulation)
- The region in the centre of the solar collector (for the canal).

- Upper region declared as "Fluid" named (air confiné):

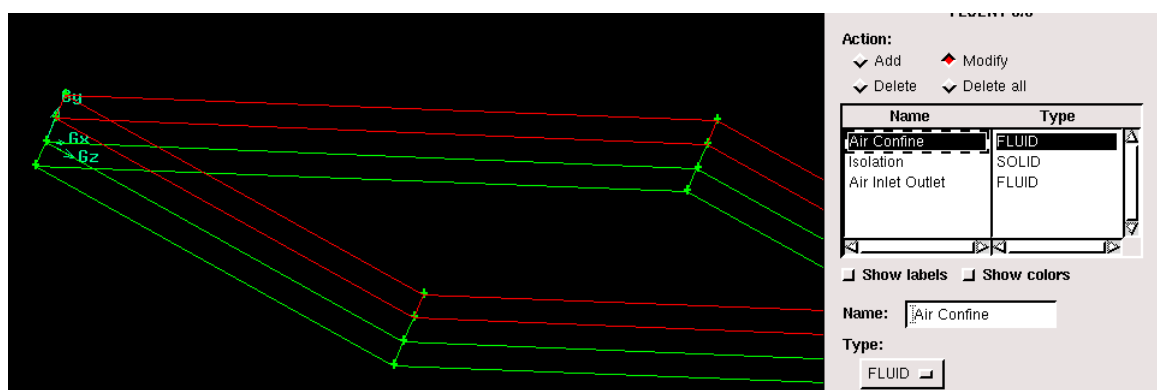


Figure 3.11: upper region of the collector

- Lower region declared as "Solid" named (isolation) :

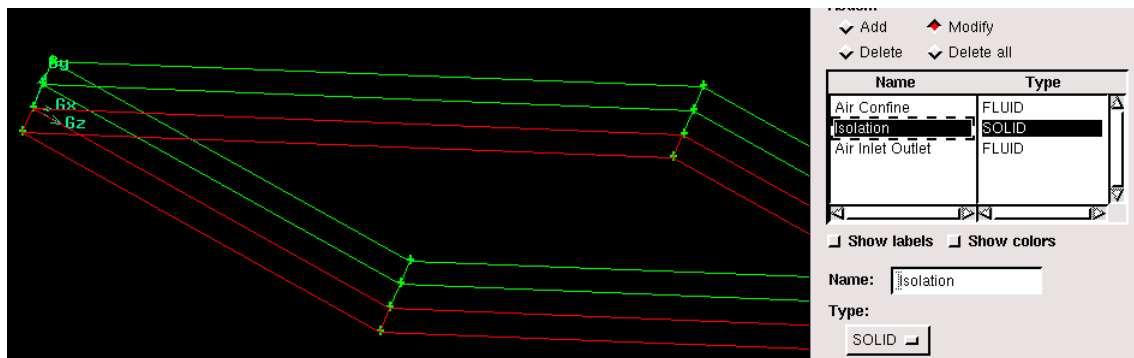


Figure 3.12: lower region of the collector

- Central region declared as "Fluid" named (Air Inlet Outlet)

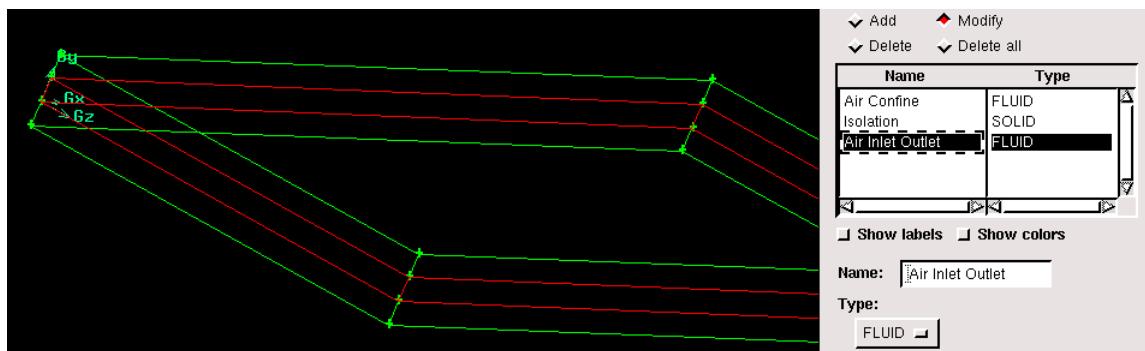


Figure 3.13: central region of the collector

3.5.3 Definition of boundary conditions :

-Glass (delclared as « wall ») :

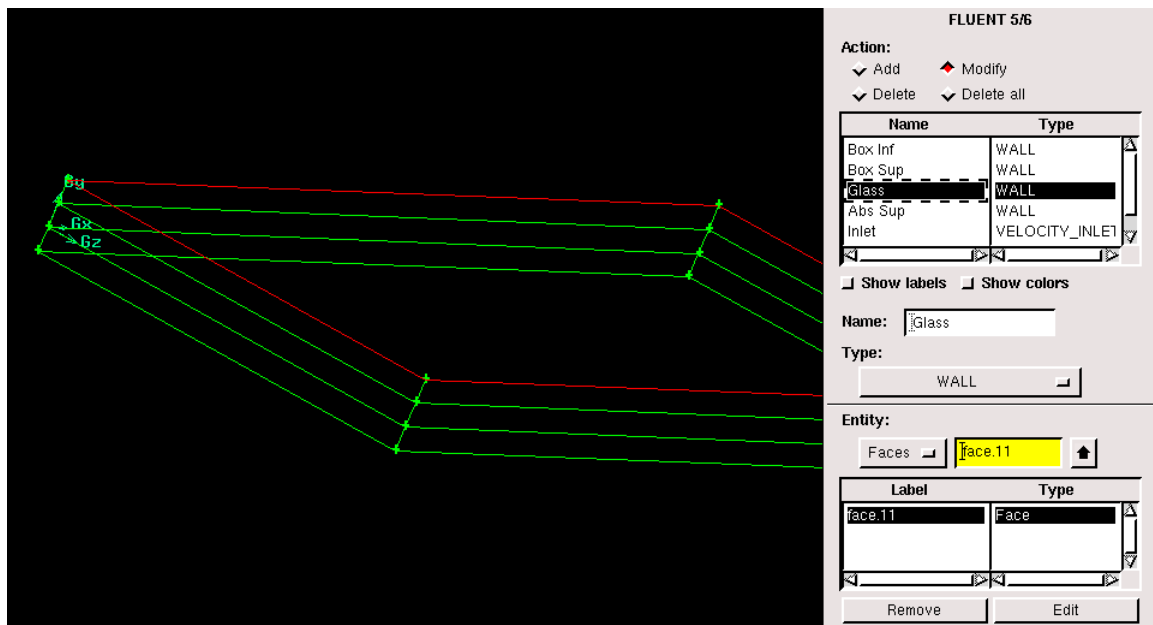


Figure 3.14: Glass as defined in gambit

-The absorbeur (declared as « wall ») :

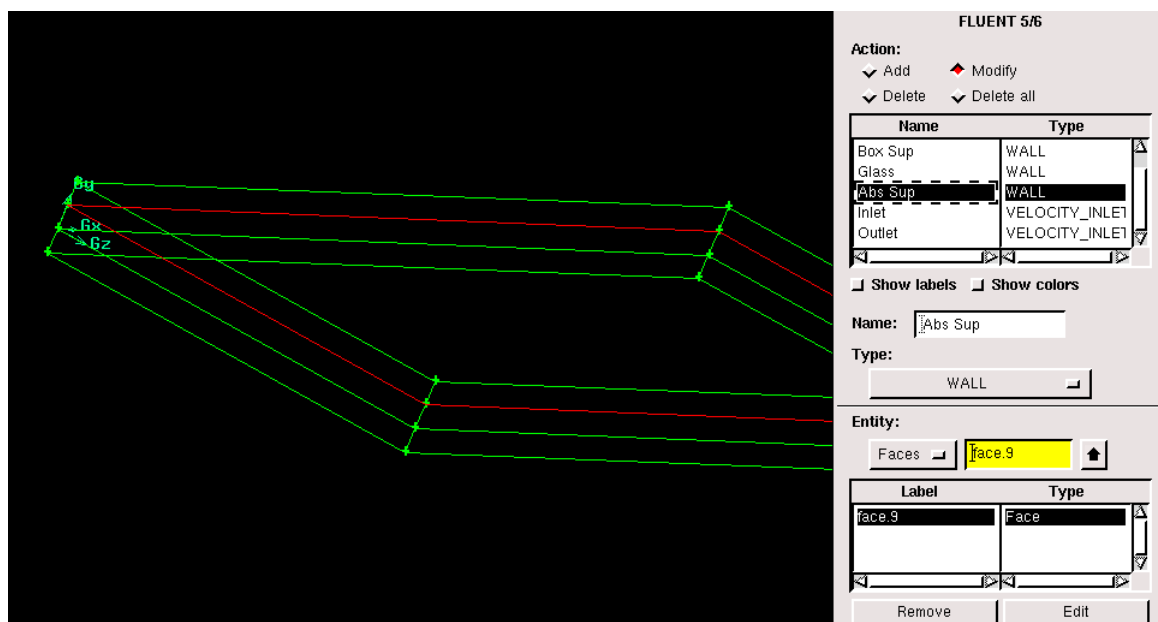


Figure 3.15: Absorber as defined in gambit

-inlet (declared as « Velocity inlet ») :

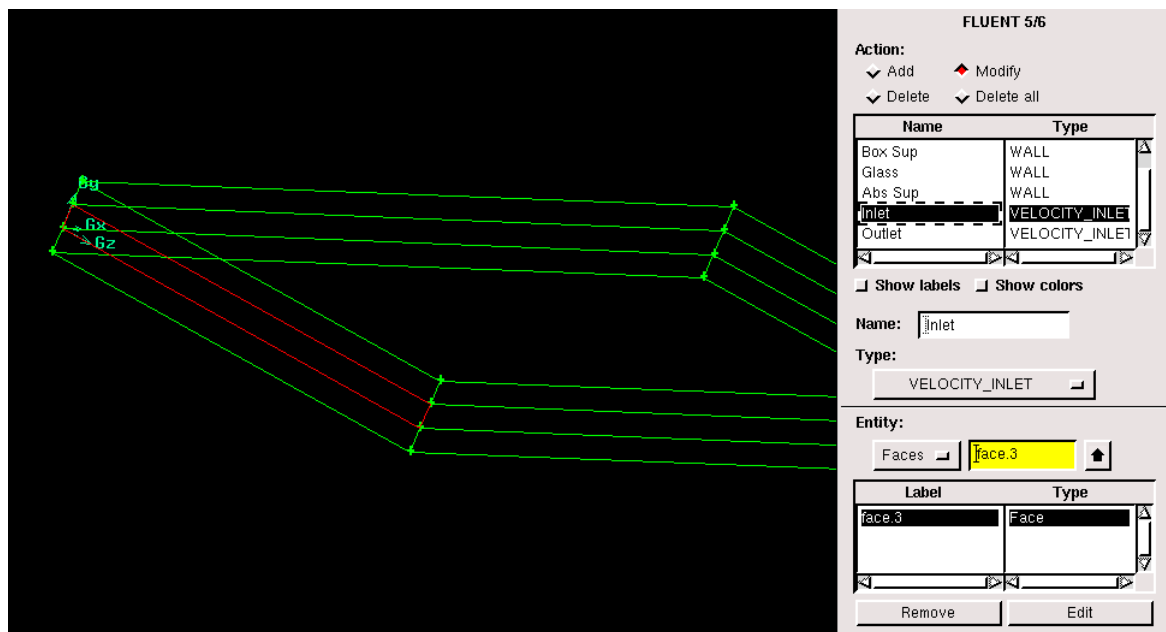


Figure 3.16: inlet as defined in gambit

- outlet (declared as « pressure outlet ») :

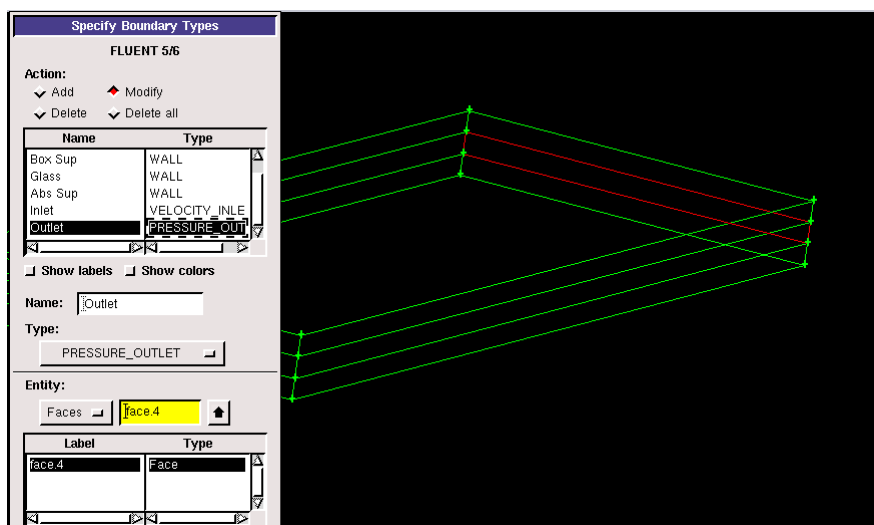


Figure 3.17: outmet as defined in gambit

3.5.4 Mesh exportation :

Once the models have been created and the boundary conditions defined, they must be exported, in .mesh format, so that Fluent is able to read them and use them to simulate their thermal and dynamic behavior. We can then close Gambit by saving the session (if we wanted to open it later) and launch Fluent.

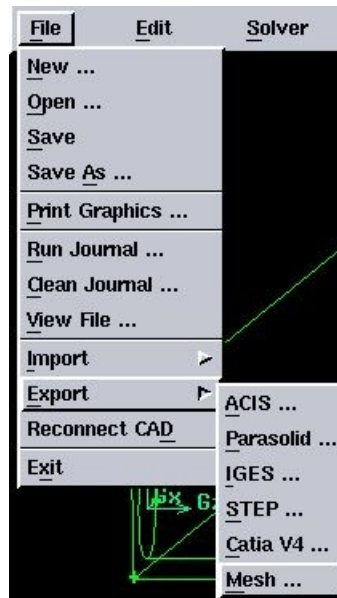


Figure 3.18: mesh exportation

Here we come to the step of using the FLUENT software, after launching the software we open the recently exported .mesh file.

3.5.5 Calculation Preparation Steps in FLUENT:

Step 1: Scale verification

This step ensures that the model is in centimeters.

Step 2 : model verification

In this step, the main parameters of the model are defined, such as the flow regime and the irradiation parameters. At the end of this step, the flow type is chosen.

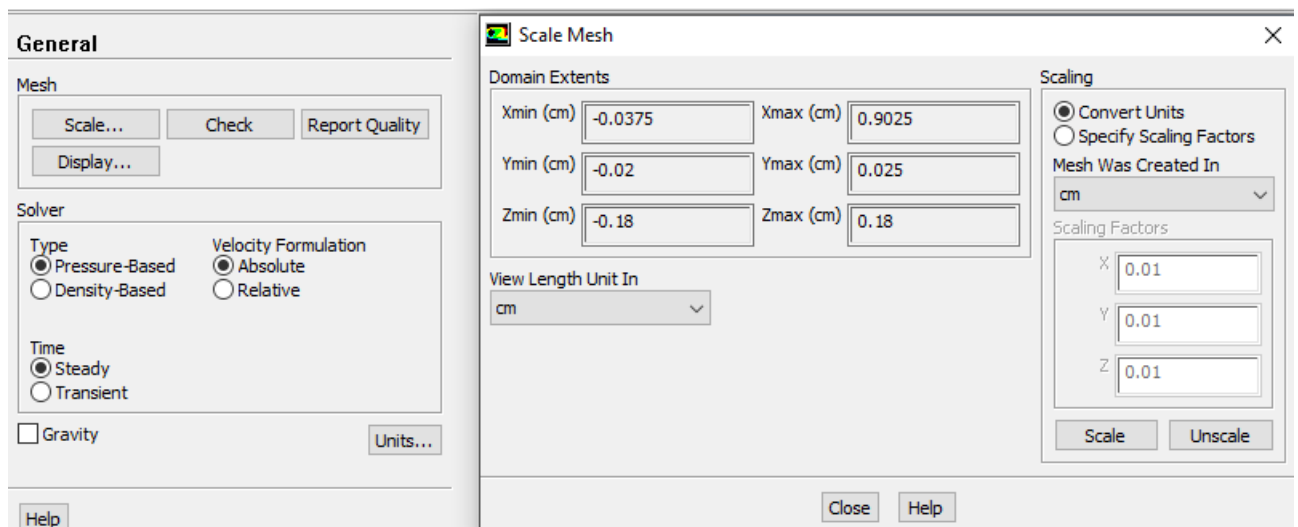


Figure 3.19: Scale verification

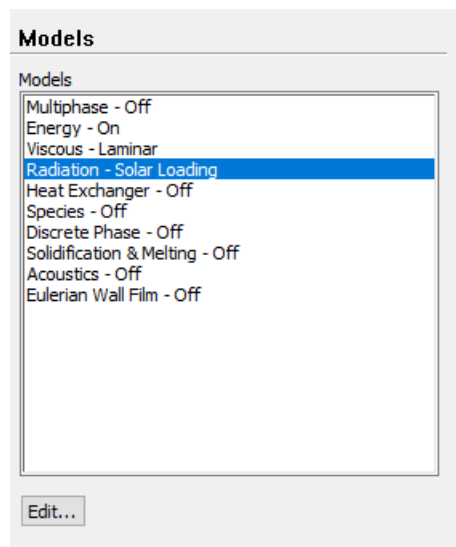


Figure 3.20: definition of model parameters

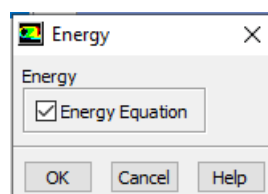


Figure 3.21: establishing the energy equations

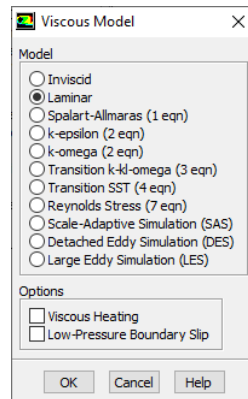


Figure 3.22: choosing « laminar » as a flow regime

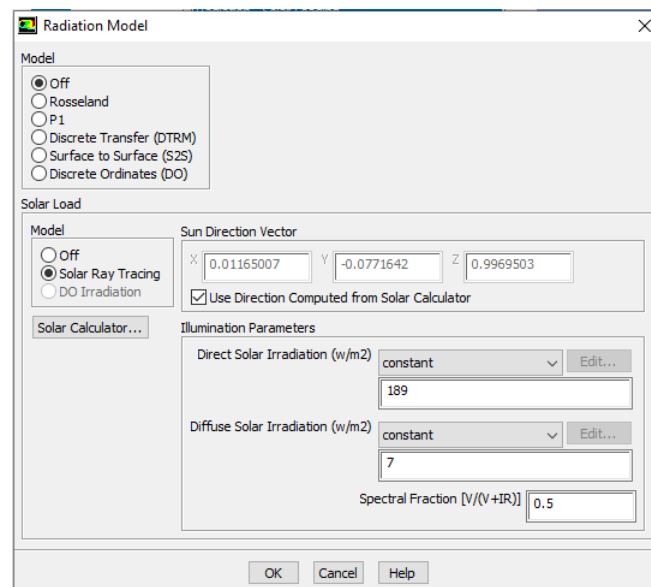


Figure 3.23: defining the radiation parameters of the model

Here, user can change the values of direct and diffuse solar irradiation based on the data he already have.

step 3 : defining the properties of materials

All thermo-physical data must be entered. The characteristics of the materials are loaded from the Fluent data library. Here we choose the materials used in our model from the existing lists, otherwise we have to introduce them according to our needs.

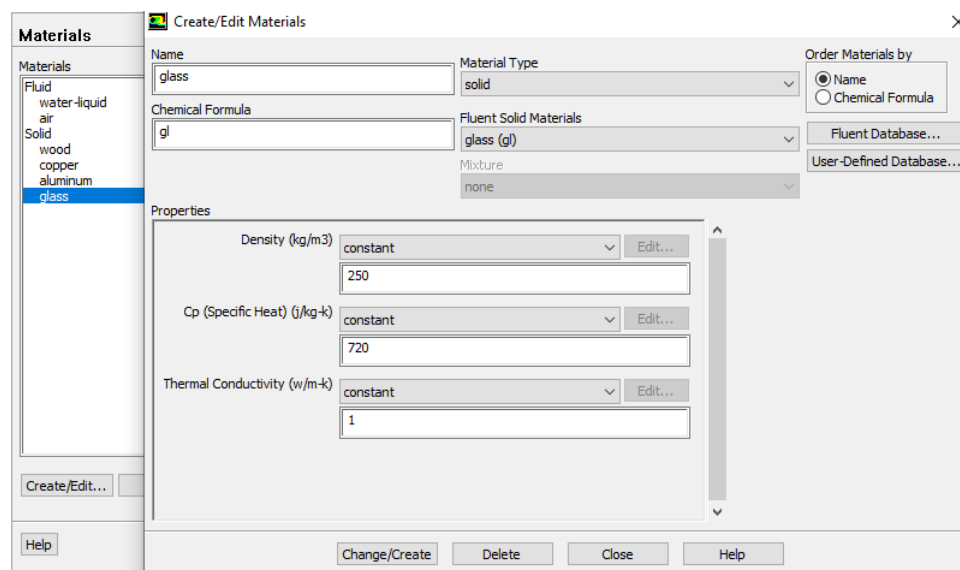


Figure 3.24: definition of a new material

The definition of a new material (glass) is given as an example:

1. The name of the solid "glass".
2. thermal density 250 kg.m-3 .
3. specific heat 720 J.Kg-1.K-1 .
3. thermal conductivity is defined through the data of the most used collectors in the market.

Step 4 : defining boundary conditions

One of the most important parameters in our study is the mass flow inlet and the inlet temperature, which can be defined through the following window:

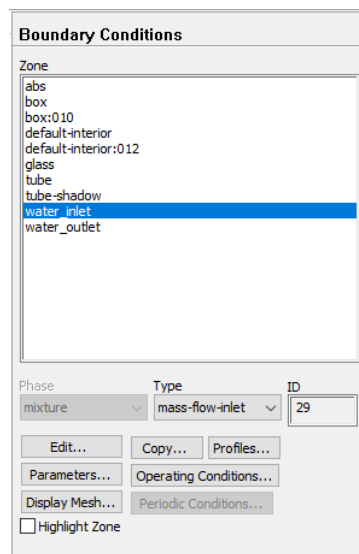


Figure 3.25: Setting boundary conditions

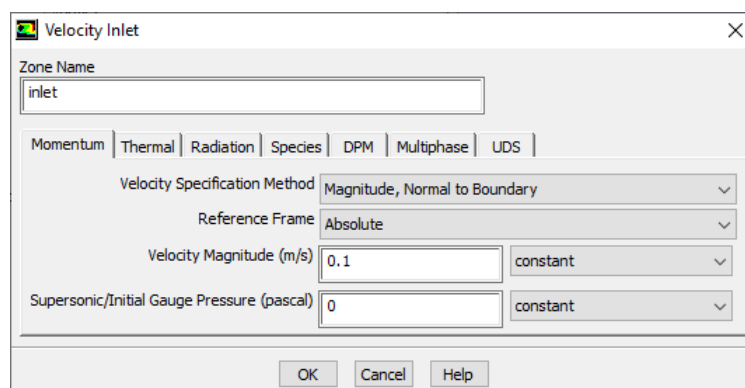


Figure 3.26: Setting the velocity inlet value

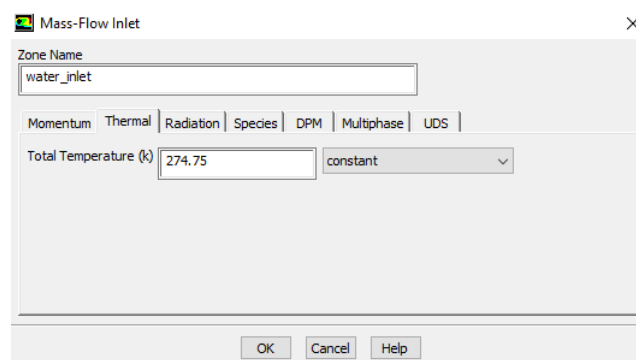


Figure 3.27: Setting the inlet temperature

Solution initialization

it is required to initialize all variables before starting the calculations. Taking into account our imposed conditions, we start the calculations at the collector's inlet.

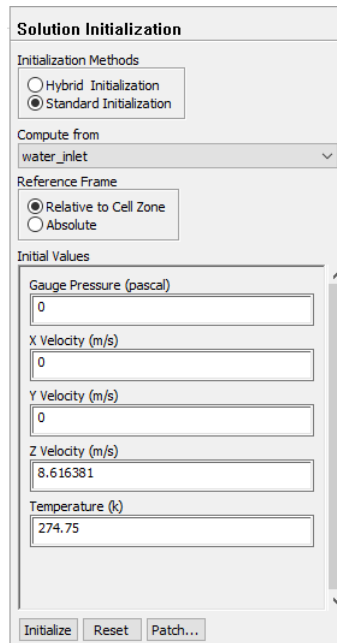


Figure 3.28: Solution initialization

start of calculation

After deciding on the number of iterations, the calculations begin.

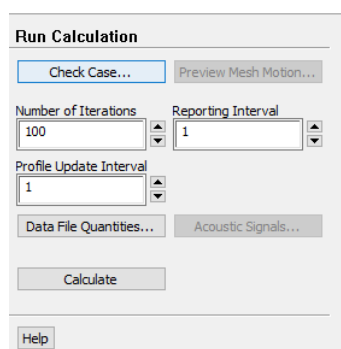


Figure 3.29: Starting calculations

3.6 Gambit and Fluent simulation tools

3.6.1 Gambit

Gambit is a software which allows to create meshes which can be used in particular under **FLUENT**.

The mesher is a preprocessing of the simulation software. It allows to generate a structured or unstructured mesh in Cartesian, polar cylindrical or axisymmetric coordinates. It can produce complex meshes in two or three dimensions It can produce complex two- or three-dimensional meshes with rectangular or triangular mesh shapes. It can be used to construct a geometry and generate a mesh for it, eventually, geometry from another CAD program can be imported into this preprocessor. preprocessor. Gambit's generation options offer flexibility of choice. It is possible to devide the geometry into several parts to generate a structured mesh. Otherwise, Gambit generates an unstructured maillage based on the type of geometry built. Defects are easily detected using the mesh verification tools.

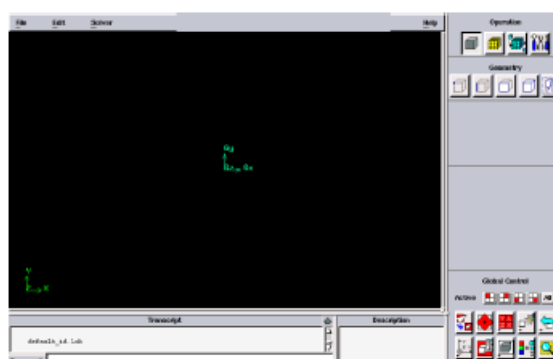


Figure 3.30: Gambit's interface

Construction of a mesh

To build a mesh, the following steps should be followed: The geometry includes the physical positions of characteristic points defining the area to be meshed: spatial coordinates of the four corners of a square, the start and end points of a line, the centre and angular opening of a circular arc. It is necessary to be able to represent the

area to be studied by a set of simple geometrical figures connected to each other.

Gambit's user guide

This software is used to define and create the study model (surface or volume) and to mesh it according to the user's instructions. The different steps to use GAMBIT are defined in the following instructions.

a. Operation tool window

Each button in this window corresponds to a well-defined function.

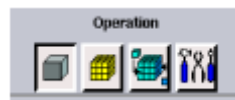


Figure 3.31: operation tool window

b. Construction of geometry

Geometry is created from points, sides, areas, volumes or a group of all of these. It is possible to perform union, intersection, separation, deletion decomposition.

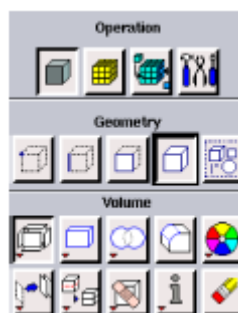


Figure 3.32: geometrie construction window

c. Mesh generation

This function allows the generation of all types of meshes, the manipulation of the generated mesh and even the creation of a boundary layer if required.



Figure 3.33: geometrie generation window

d. Incorporation of boundary conditions

Several types of boundary conditions are available depending on the problem being addressed. Note that that the mesh space is taken by default as being fluid.



Figure 3.34: boundary conditions definition buttons

e. Tools buttons

They allow to specify the coordinate system for example or other specific operations.



Figure 3.35: tools buttons

f. Global control window

It concerns orientation, display, light and mesh checking.



Figure 3.36: global control window

Important : Even before creating the geometry, it is necessary to choose the type of solver; in other words, the type of software (here Fluent) that will be used afterwards (choose the right version of the software), in our case it is to choose Fluent 5/6.

3.6.2 Fluent code

Fluent is a computer program designed for the simulation of fluid flow and heat transfer in complex geometries. It offers great flexibility of results and adaptation with any type of mesh. It allows the refinement of the mesh according to boundary conditions, dimensions and even results already obtained. This is very useful in the region of high gradients (boundary layers, free shear layers). Fluent is written in the C language and uses all the flexibility and power that this language offers. It uses the client-server architecture necessary for parallel computing on multiple machines. Fluent has a graphical tool for displaying and evaluating the results. Results can also be exported to other graphics software, and the user defined function option allows additional equations or additional user-defined source terms to be solved.

Interface of the Fluent code:

We can start 4 versions of Fluent 2D, 3D, 2DDP and 3DDP with the same interface.

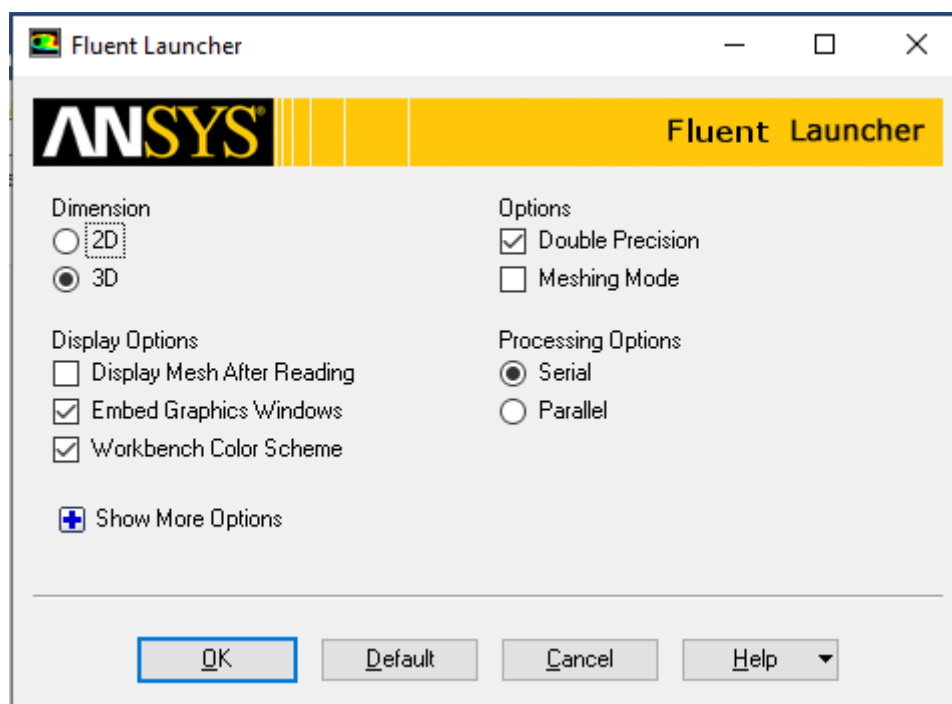


Figure 3.37: Fluent launcher window

The functions available for the digital procedure are :

File: for operations concerning files: reading, saving, importing, etc.

Grid: for checking and manipulating the mesh and geometry.

Define: for defining physical phenomena, materials and boundary conditions.

Solve: to choose the equations to be solved, the discretization schemes, the sub-relaxation factors, the convergence criteria and to initialize and proceed with the calculation.

Adapt: to adapt the mesh according to several parameters.

Surface: to create points, lines and planes necessary to display the results.

Display and plot: for the evaluation of the results. **Report:** for displaying reports containing details of the problem processed.

Parallel: for parallel calculation.

Help: for the exploitation of the code content.

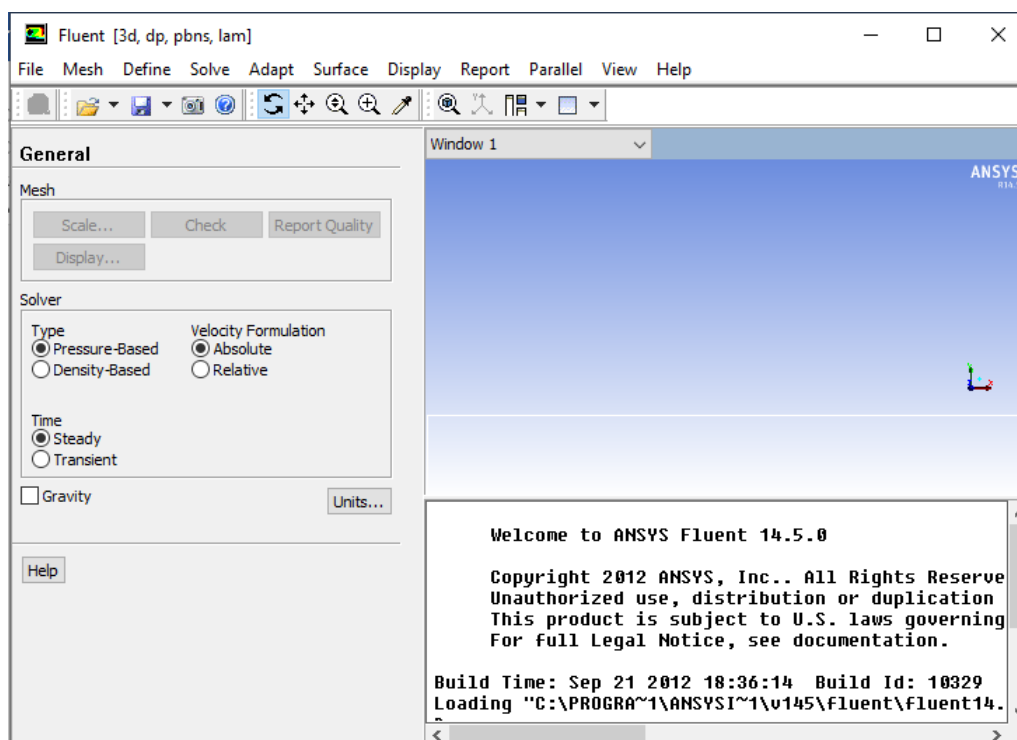


Figure 3.38: Fleunt interface

Boundary condition used by the Fluent code :

For the Fluent code the available types of boundary conditions are classified as follows:

- a) **Flow inlet and outlet conditions:** pressure inlet, velocity inlet, mass flow inlet, intake, pressure outlet, outflow, pressure far-field, exhaust.
- b) **Wall and pole condition:** wall, axis of symmetry, periodic conditions, plane of symmetry.
- c) **Internal zone cells:** fluid or solid (of different types).
- d) **Condition of the internal faces:** ventilation, radiation, internal wall.

But if we speak in a more general way we will have four types of boundary conditions or each of them needs a thorough study:

- At the inlet:** the value of the variable is known.
- At the outlet:** either the value of the given variable is known or it is assumed that the regime is established.
- At the wall:** either the variable is known (e.g. velocity or temperature), or other physical quantities are known (velocity gradient, heat flow).

-On the axis of symmetry: where the gradient of the posed variable in the direction perpendicular to the axis of symmetry is zero.

Numerical model used by the Fluent code:

The Fluent code uses the finite volume method to discretise the transport equations. In this method, conservation equations are integrated and applied to each elementary control volume. From the known variables at the centres of the volumes, the flows at the surfaces of the volumes are evaluated by interpolation. The grid is a priori arbitrary, thus allowing to treat flows with complex geometry. This method gives very good results, because it guarantees the conservation of the mass and heat balances over the whole studied domain.

3.7 conclusion

This chapter has been dedicated to the description of the numerical modelling approach we have used for the problem to be solved. We started by presenting the geometry of the system. We then set out the set of governing equations and the associated simplifying assumptions and boundary conditions, in relation to the heat and mass transport within the sensor. This chapter ends with a brief description of the Gambit and Fluent software and the steps to follow to explain the simulation that was done to obtain the results that will be presented in the next chapter. In the following chapter, we will present the results obtained from the numerical simulation and their interpretations.

Chapter 4

Results and discussion

4.1 Introduction

This chapter is dedicated to the presentation of various numerical results obtained with ANSYS-FLUENT 14.5 software, using real data acquired during an internship performed at the Research Unit for Renewable Energies in the Saharan Environment (URER-MS) in Adrar.

The goal of this study is to numerically simulate the thermal behaviour of air passing through a rectangular channel of a flat plate solar collector. The low heat exchange between the heat transfer fluid and the absorber leads us to investigate other ways to improve the efficiency of the collector, for which it was quite useful to study the geometrical shape, the dimensioning and the velocity of the fluid passing inside the solar collector.

In this work, we will choose to study a flat plate air collector intended in our case for a solar dryer. The required parameters used in the numerical simulation are obtained from the URER-MS daily archive for the 5th of January 2020 in the Adrar region.

First, we will test several air inlet velocities existing in the current literature and in the external market as being velocities often used in the design of flat plate air collectors, in order to see the influence of the inlet velocity on the heat transfer

between the absorbing wall and the air flowing in the collector channel. Next, we will check the evolution of the air temperature profile throughout the day.

4.2 Results and discussion

In this work, we will focus on the heat transfer between the absorbing wall and the air passing through the solar collector channel in stationary regime for the day of January 5, 2020 in the Adrar region.

4.2.1 Evolution of air temperature profiles for different inlet velocities

In order to see the influence of the airflow velocity through the collector canal on the evolution of its temperature by exchanging heat with the absorber, four velocity profiles were examined (0.3 m/s, 0.1 m/s, 0.08 m/s and 0.05 m/s) with the maximum daytime temperature of 5 January 2020 in the Adrar region ($T_{amb} = 293.15$ K, $D_i = 903$ W/m², $D_H = 55$ W/m²).

a/ For an airflow velocity of 0.3 m/s

Figure 5.1 shows the evolution of the air temperature profiles inside the central part of the collector (between the thermal insulation and the absorber plate) on an (X,Z) plane in the middle of the solar collector, for an air inlet velocity of 0.3 m/s and an inlet temperature of 294 K. The result shows that the air temperature increases progressively in the (X, Z) direction due to the convective heat exchange between the absorber and the air flowing in the channel. It can also be seen that the absorber receives energy from the greenhouse effect in the upper part where the air is confined. At the exit of the channel, the air reaches a temperature of 299 K. So it leaves with a gain of almost 5 degrees.

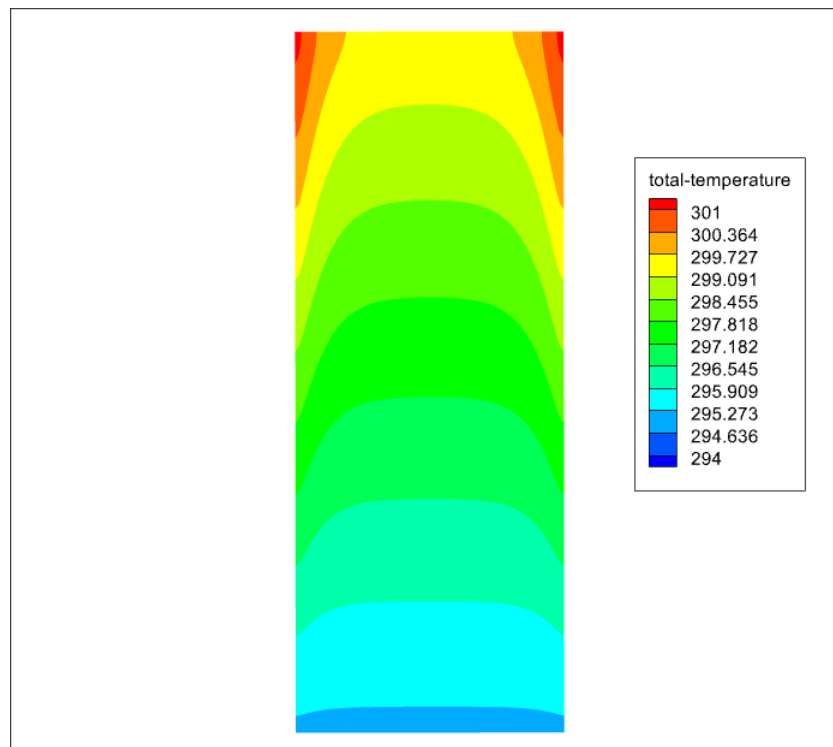


Figure 4.1: Evolution of the (X, Z)-temperature profiles of the air for an inlet velocity of 0.3 m/s.

b/ For an airflow velocity of 0.1 m/s :

Figure 5.2 shows the evolution of the air temperature profiles inside the central part of the collector (between the thermal insulation and the absorber plate) on an (X,Z) plane in the middle of the solar collector, for an air inlet velocity of 0.1 m/s and an inlet temperature of 294 K. At the exit of the channel, it can be seen that the air reaches a temperature of 310 K. So the air has received more energy compared to the inlet speed of 0.3 m/s. This means a gain of 16 degrees.

c/ For an airflow velocity of 0.08 m/s :

Figure 5.3 shows the evolution of the air temperature profiles inside the central part of the collector (between the thermal insulation and the absorber plate) on an (X,Z) plane in the middle of the solar collector, for an air inlet velocity of 0.08 m/s and an inlet temperature of 294 K. At the exit of the channel, it can be seen that the air reaches a temperature of 314 K. Therefore the air leaves the channel with a gain of 15 degrees compared to the speed of 0.3 m/s and a gain of 4 degrees compared to the

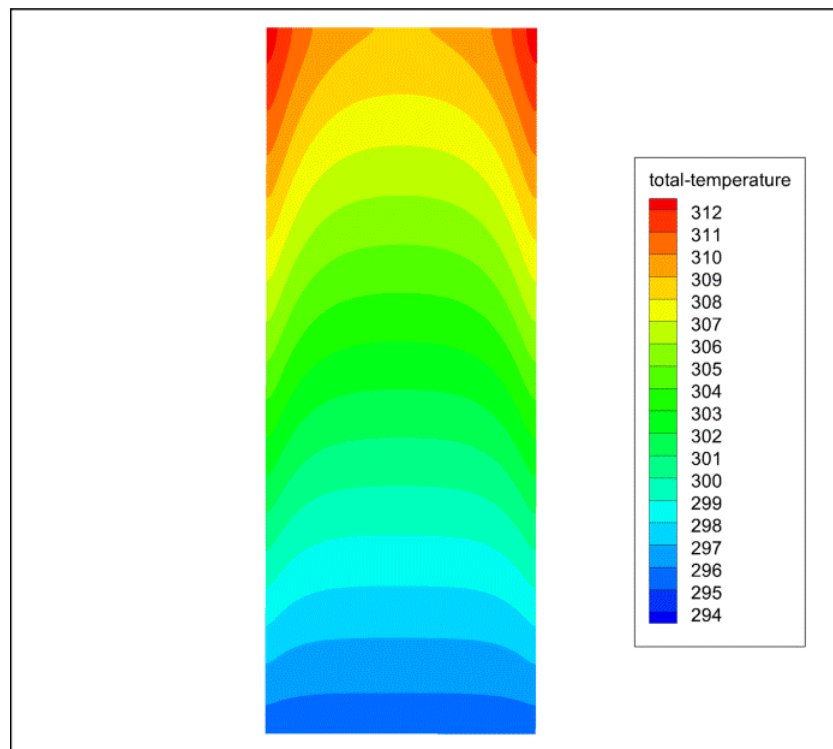


Figure 4.2: Evolution of the (X, Z)-temperature profiles of the air for an inlet velocity of 0.1 m/s.

speed of 0.1 m/s.

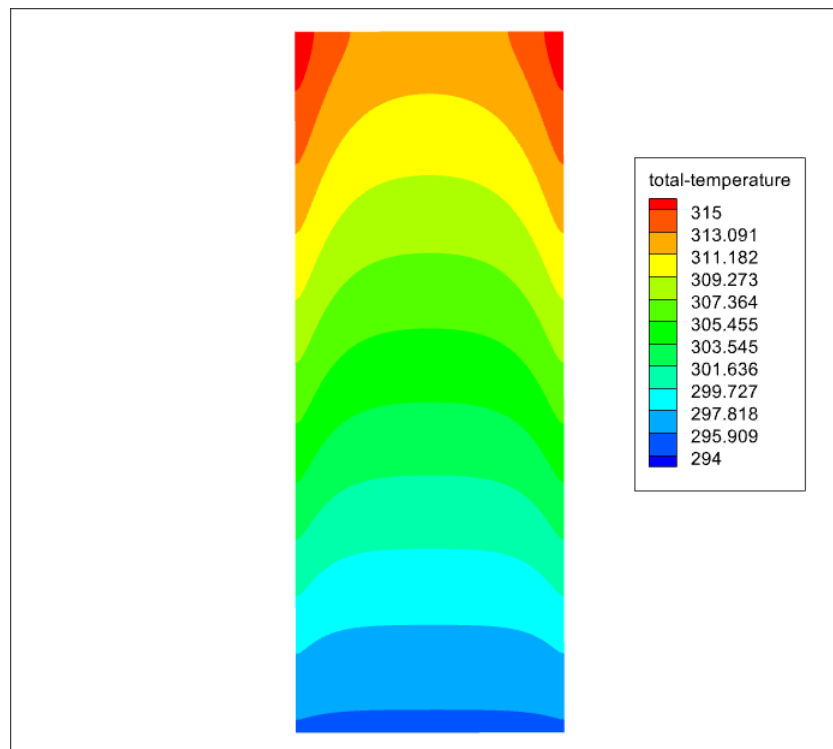


Figure 4.3: Evolution of the (X, Z) -temperature profiles of the air for an inlet velocity of 0.08 m/s.

d/ For an airflow velocity of 0.05 m/s :

Figure 4.4 shows the evolution of the air temperature profiles inside the central part of the collector (between the thermal insulation and the absorber plate) on an (X, Z) plane in the middle of the solar collector, for an air inlet speed of 0.05 m/s and an inlet temperature of 294 K. At the exit of the channel, we notice that the air reaches a temperature of 323 K. Therefore the air leaves the channel with a gain of 29 degrees, 24 degrees compared to the speed of 0.3 m/s, a gain of 13 degrees compared to the speed of 0.1 m/s, and a gain of 9 degrees compared to the speed of 0.08 m/s

The results obtained from the numerical simulation for the four proposed velocities (0.3 m/s, 0.1 m/s, 0.08 m/s and 0.05 m/s) highlight the influence of the air flow velocity on its temperature, as the heat transfer between the absorber plate and the air in the canal becomes increasingly important as the air passes slowly through the canal. In the present work, we will choose the inlet velocity of 0.05 m/s for the further calculation of the evolution of the (X, Z) -temperature profiles of the air during

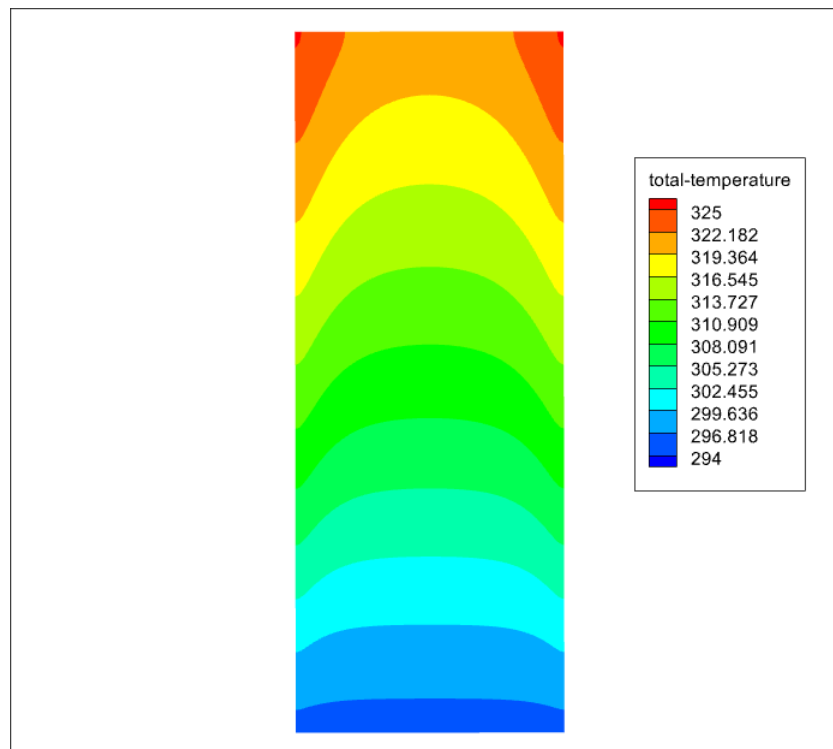


Figure 4.4: Evolution of the (X, Z)-temperature profiles of the air for an inlet velocity of 0.05 m/s.

the twenty-four hours. Because it provides the best performance.

4.2.2 Evolution of air temperature profiles during the day

Evolution of air temperature profiles during the day of January 5, 2020 in the Adrar region were simulated for an inlet velocity of 0.05 m/s which represents the optimal inlet velocity calculated previously.

a/ 08 h 00 ($T_{amb} = 274,75$ K, $D_i = 189$ W/m², $DH = 7$ W/m²)

Figure 5.5 shows the evolution of the air temperature profiles inside the central part of the collector (between the insulation and the absorber plate) on an (X, Z) plane in the middle of the solar collector, for an air inlet velocity of 0.05 m/s at 08:00 a.m., where the ambient temperature $T_{amb} = 274.75$ K, the direct normal irradiation $D_i = 189$ W/m², and the diffuse horizontal irradiation $DH = 7$ W/m².

It can be seen that the air enters the channel with a temperature of 274.75 K, the temperature of the air in the canal increases slightly in the x- and z-direction until it

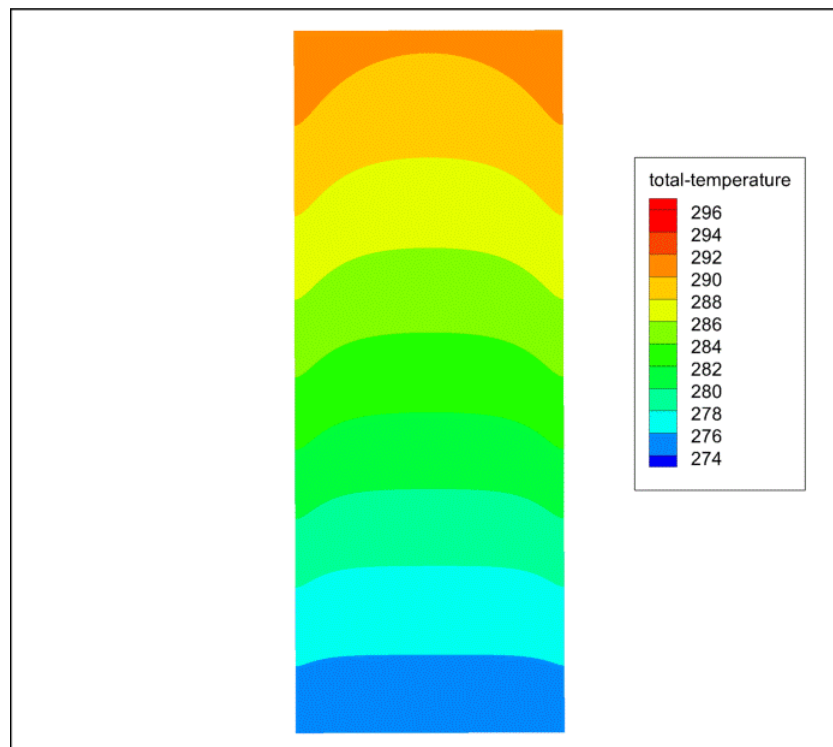


Figure 4.5: Evolution of the (X, Z) -air temperature profiles for an inlet velocity of 0.05 m/s at 08:00 ($T_{amb} = 274.75$ K , $D_i = 189$ W/m², $DH = 7$ W/m²)

arrives at the exit with a temperature of (292 K), so the air exits the canal with a gain of almost 17 degrees at this period because the solar radiation is not strong enough at the beginning of the day.

b/ 10 h 00 ($T_{amb} = 278,95$ K , $D_i = 922$ W/m², $DH = 49$ W/m²)

Figure 5.6 shows the evolution of the air temperature profiles inside the central part of the collector (between the insulation and the absorber plate) on an (X, Z) plane in the middle of the solar collector, for an air inlet velocity of 0.05 m/s at 10:00 a.m., where the ambient temperature $T_{amb} = 278.95$ K, the direct normal irradiation $D_i = 922$ W/m², and the diffuse horizontal irradiation $DH = 49$ W/m².

We observe that the air enters the channel with a temperature of 278.95 K, the temperature of the air in the canal increases progressively in the x - and z -direction until it arrives at the exit with a temperature of (309 K), so the air leaves the collector with a gain of almost 31 degrees at this time because the solar radiation has not yet reached the maximum but it offers us a better performance than at 8:00 am.

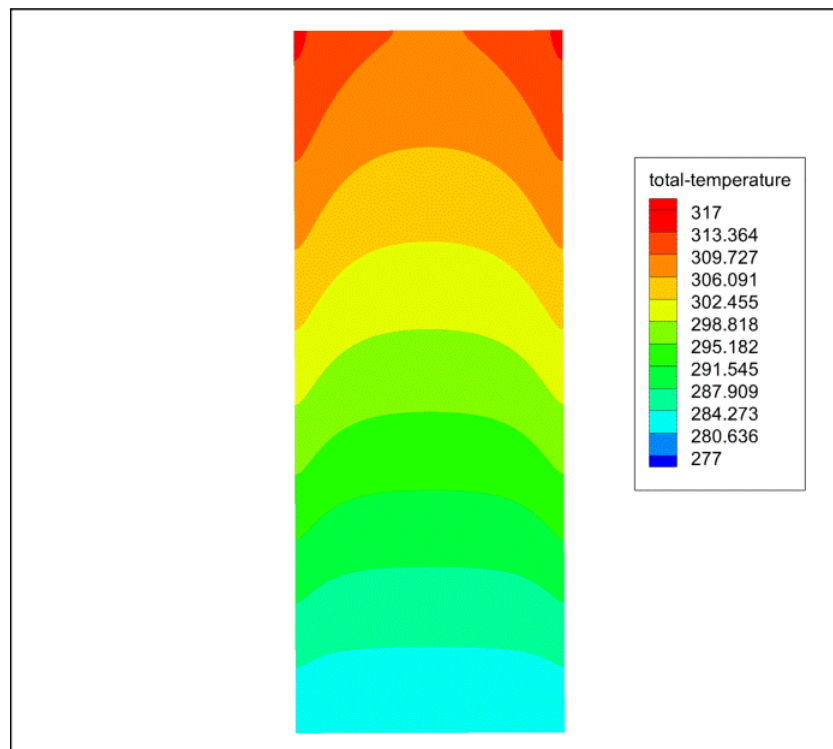


Figure 4.6: Evolution of the (X, Z)-air temperature profiles for an inlet velocity of 0.05 m/s at 10 h 00 ($T_{amb} = 278,95$ K, $D_i = 922$ W/m², $DH = 49$ W/m²)

c/ 12 h 00 ($T_{amb} = 285, 95$, $D_i = 1025$ W/m², $DH = 60$ W/m²)

Figure 5.7 shows the evolution of the air temperature profiles inside the central part of the collector (between the insulation and the absorber plate) on an (X,Z) plane in the middle of the solar collector, for an air inlet velocity of 0.05 m/s at 12.00 a.m., where the ambient temperature $T_{amb} = 285.95$ K, the direct normal irradiation $D_i = 1025$ W/m², and the diffuse horizontal irradiation $DH = 60$ W/m².

It can be seen that the air enters the collector with a temperature of 285.95 K, the temperature of the air in the canal increases slightly in the x- and z-direction until it arrives at the outlet with a temperature of (321 K), so the air leaves the canal with a gain of almost 35 degrees at this time, so it gives us a better performance than at 10:00 am, which is satisfying.

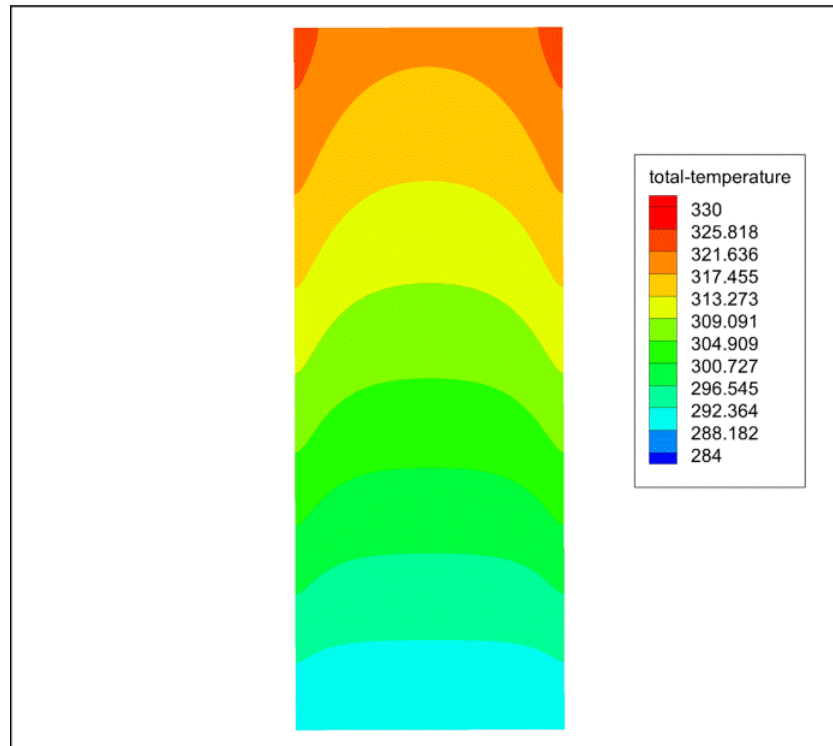


Figure 4.7: Evolution of the (X, Z)-air temperature profiles for an inlet velocity of 0.05 m/s at 12 h 00 ($T_{amb} = 285, 95$, $D_i = 1025 \text{ W/m}^2$, $DH = 60 \text{ W/m}^2$)

d/ 13 h 30 ($T_{amb} = 289, 95$, $D_i = 1044 \text{ W/m}^2$, $DH = 60 \text{ W/m}^2$)

Figure 5.8 shows the evolution of the air temperature profiles inside the central part of the collector (between the insulation and the absorber plate) on an (X,Z) plane in the middle of the solar collector, for an air inlet velocity of 0.05 m/s at 13:30, where the ambient temperature $T_{amb} = 289.95 \text{ K}$, the direct normal irradiation $D_i = 1044 \text{ W/m}^2$, and the diffuse horizontal irradiation $DH = 60 \text{ W/m}^2$ It can be seen that the air enters the canal with a temperature of 289.95 K, the temperature of the air in the collector increases slightly in the x- and z-direction until it reaches the outlet with a temperature of (323 K), so the air leaves the canal with a gain of almost 33 degrees at this time, which is the maximum gain achieved so far.

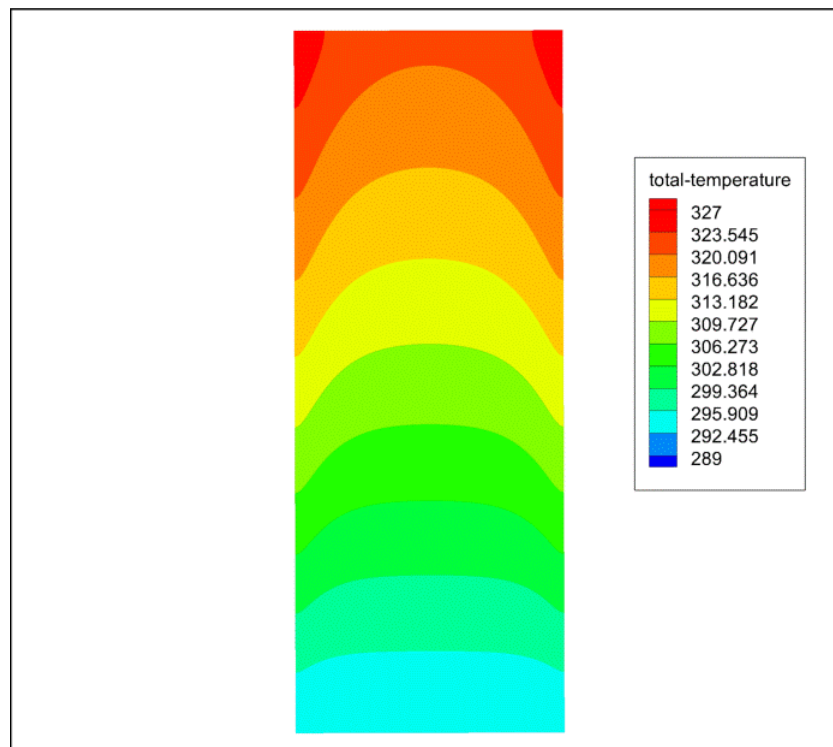


Figure 4.8: Evolution of the (X, Z)-air temperature profiles for an inlet velocity of 0.05 m/s at 13 h 30 ($T_{amb} = 289,95$, $D_i = 1044 \text{ W/m}^2$, $DH = 60 \text{ W/m}^2$)

e/ 14 h 00 ($T_{amb} = 291,05$, $D_i = 1037 \text{ W/m}^2$, $DH = 60 \text{ W/m}^2$)

Figure 5.9 shows the evolution of the air temperature profiles inside the central part of the collector (between the insulation and the absorber plate) on an (X,Z) plane in the middle of the solar collector, for an air inlet velocity of 0.05 m/s at 14:00, where the ambient temperature $T_{amb} = 291.05 \text{ K}$, the direct normal irradiation $D_i = 1037 \text{ W/m}^2$, and the diffuse horizontal irradiation $DH = 60 \text{ W/m}^2$ It can be seen that the air enters the sensor with a temperature of 291.05 K, the temperature of the air in the canal increases progressively in the x- and z-direction until it reaches the outlet with a temperature of (321 K), so the air leaves the canal with a gain of almost 30 degrees at this time. In which the ambient temperature is close to the maximum value of the day.

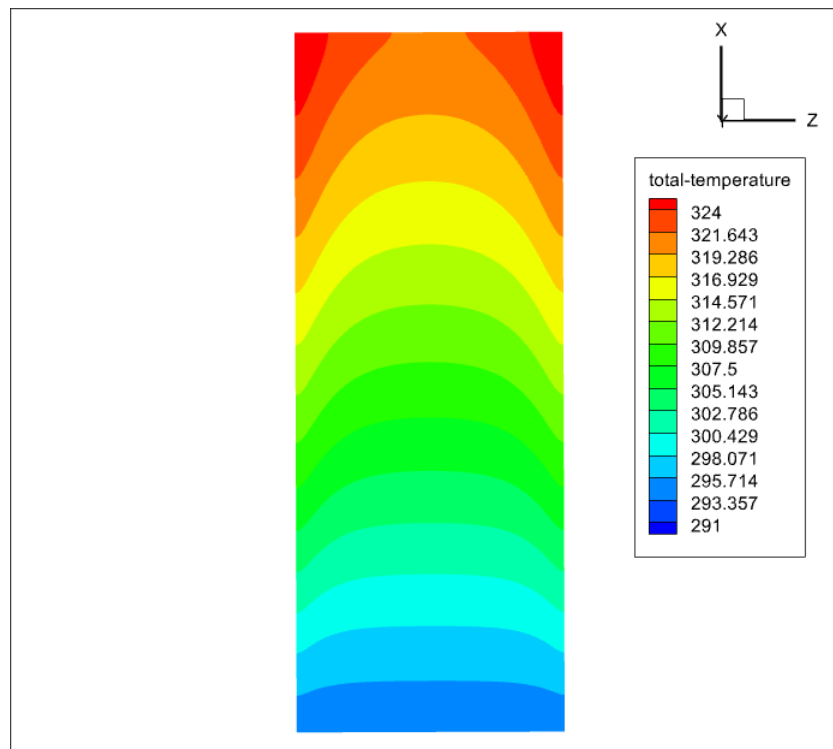


Figure 4.9: Evolution of the (X, Z)-air temperature profiles for an inlet velocity of 0.05 m/s at 14 h 00 ($T_{amb} = 291,05$, $D_i = 1037$ W/m², $DH = 60$ W/m²)

f/ 16 h 15 ($T_{amb} = 293,15$ K , $D_i = 903$ W/m², $DH = 55$ W/m²)

Figure 5.10 shows the evolution of the air temperature profiles inside the central part of the collector (between the insulation and the absorber plate) on an (X.Z) plane in the middle of the solar collector, for an air inlet velocity of 0.05 m/s at 16:15, where the ambient temperature $T_{amb} = 293.15$ K, the direct normal irradiation $D_i = 903$ W/m², and the diffuse horizontal irradiation $DH = 55$ W/m²..... It can be seen that the air enters the canal with a temperature of 293.15 K, the temperature of the air in the canal increases progressively in the x- and z-direction until it arrives at the exit with a temperature of 50°C (323 K), so the air leaves the canal with a gain of almost 30 degrees at this period in which the ambient temperature is maximum.

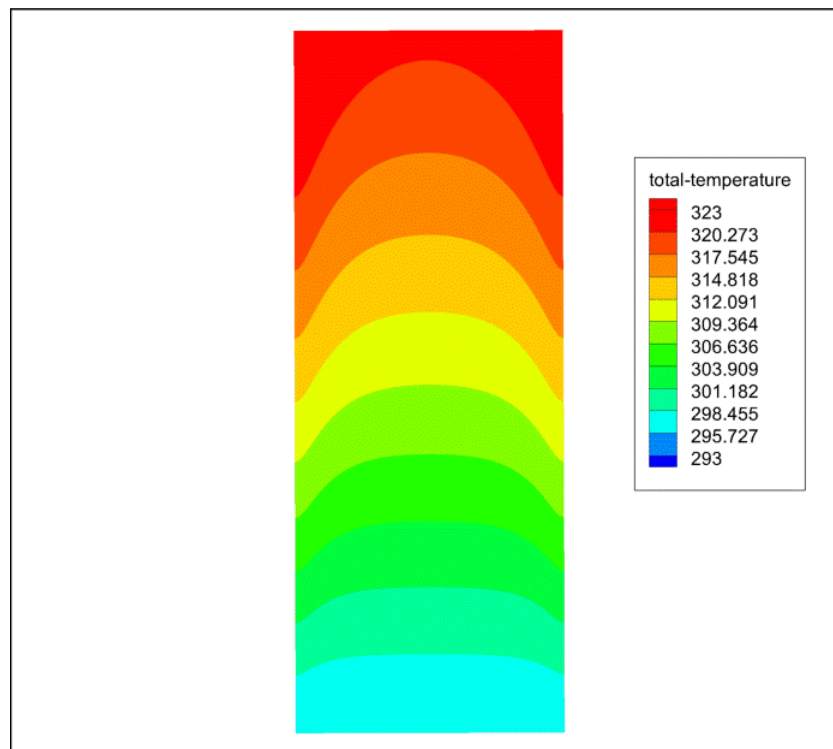


Figure 4.10: Evolution of the (X, Z)-air temperature profiles for an inlet velocity of 0.05 m/s at 16 h 15 ($T_{amb} = 293,15 \text{ K}$, $D_i = 903 \text{ W/m}^2$, $DH = 55 \text{ W/m}^2$)

g/ 20 h 00 ($T_{amb} = 286,75 \text{ K}$, $D_i = 0 \text{ W/m}^2$, $DH = 0 \text{ W/m}^2$)

Figure 5.11 shows the evolution of the air temperature profiles inside the central part of the collector (between the insulation and the absorber plate) on an (X,Z) plane in the middle of the solar collector, for an air inlet velocity of 0.05 m/s at 20:00, or the ambient temperature $T_{amb} = 286.75 \text{ K}$, the direct normal irradiation $D_i = 0 \text{ W/m}^2$, and the diffuse horizontal irradiation $DH = 0 \text{ W/m}^2$ It can be seen that the air enters the collector with a temperature of 286.75 K, the temperature of the air in the canal increases slightly in the x- and z-direction until it arrives at the exit with a temperature of (294 K), so the air leaves the canal with a gain of almost 7 degrees at this period in which the ambient temperature is low and the radiation is nil because it is night.

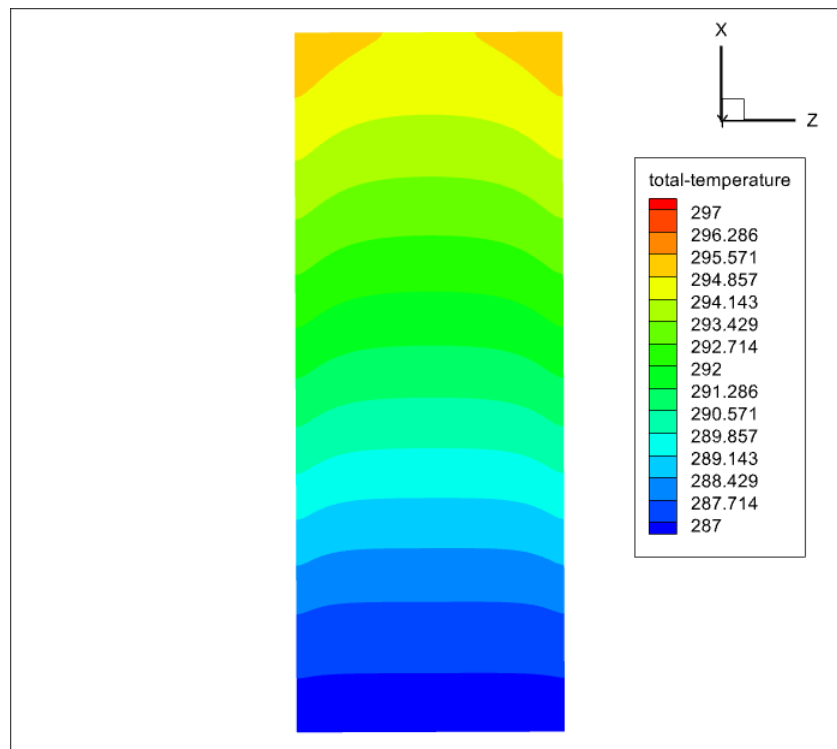


Figure 4.11: Evolution of the (X, Z)-air temperature profiles for an inlet velocity of 0.05 m/s at 20 h 00 ($T_{amb} = 286,75$ K, $D_i = 0$ W/m², $D_H = 0$ W/m²)

During the twenty-four hours, it can be said that the flat plate air collector reaches the best efficiency at midday (12:00) with a gain of 35 degrees as illustrated in the following figures:

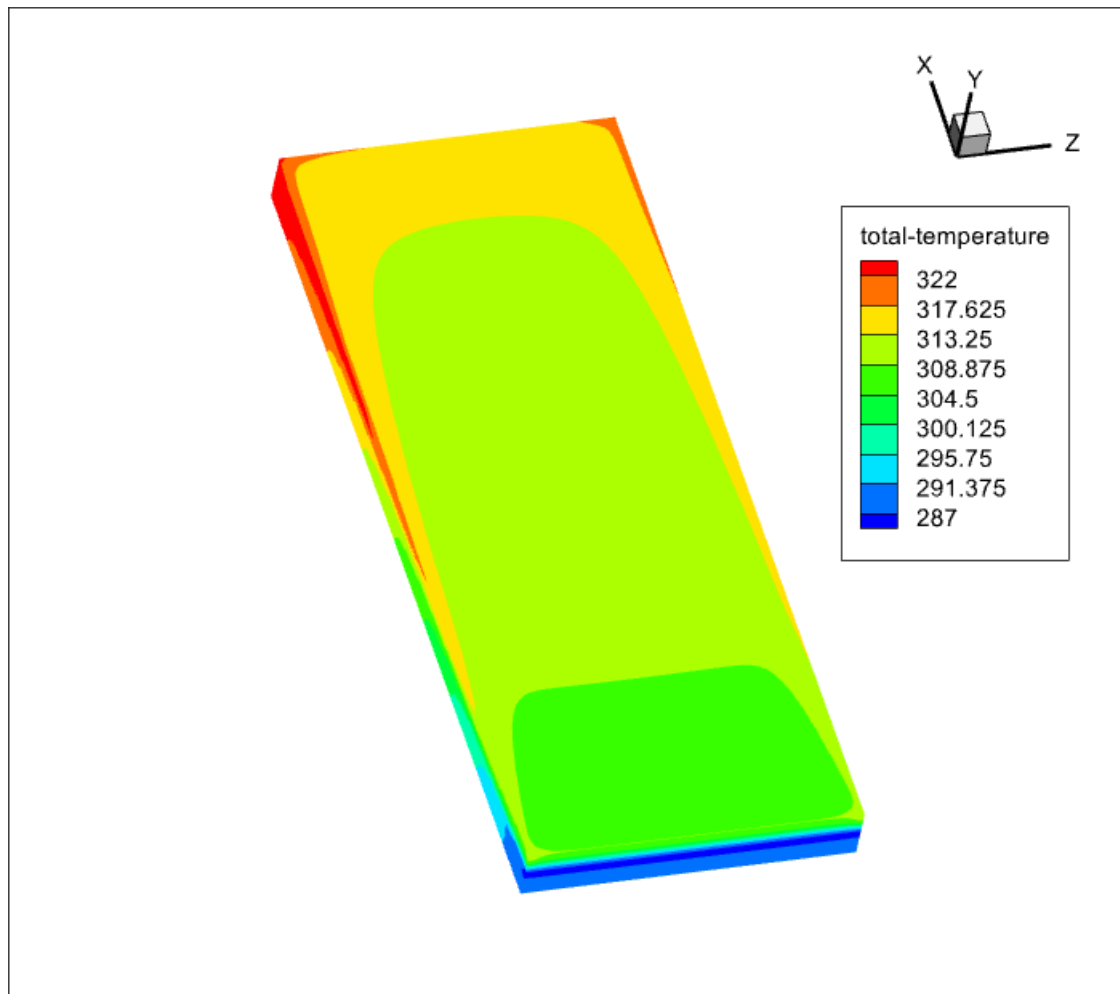


Figure 4.12: Distribution of the temperature evolution on the solar collector box at 12:00

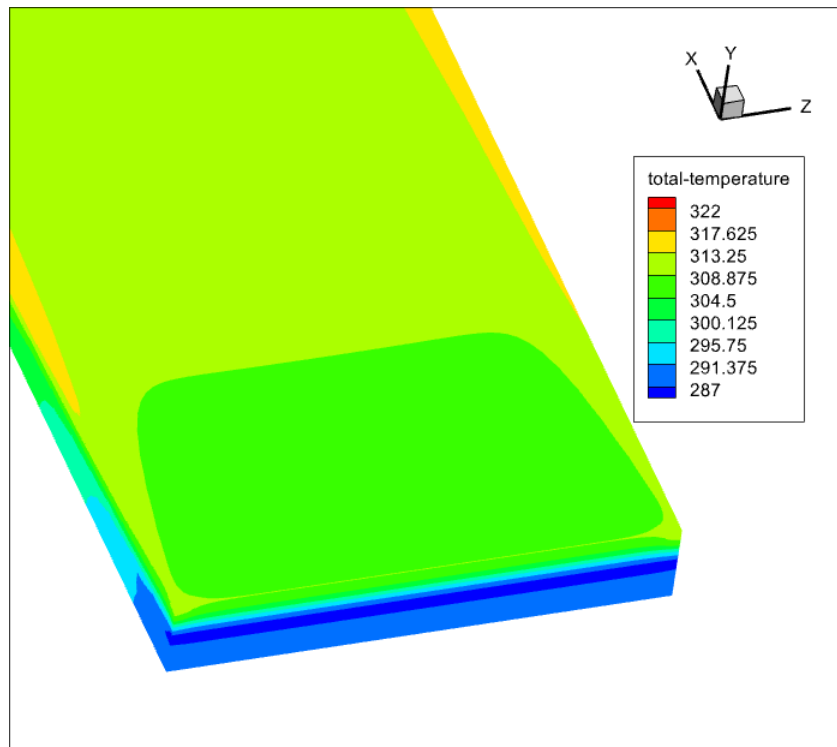


Figure 4.13: Inlet at 12:00

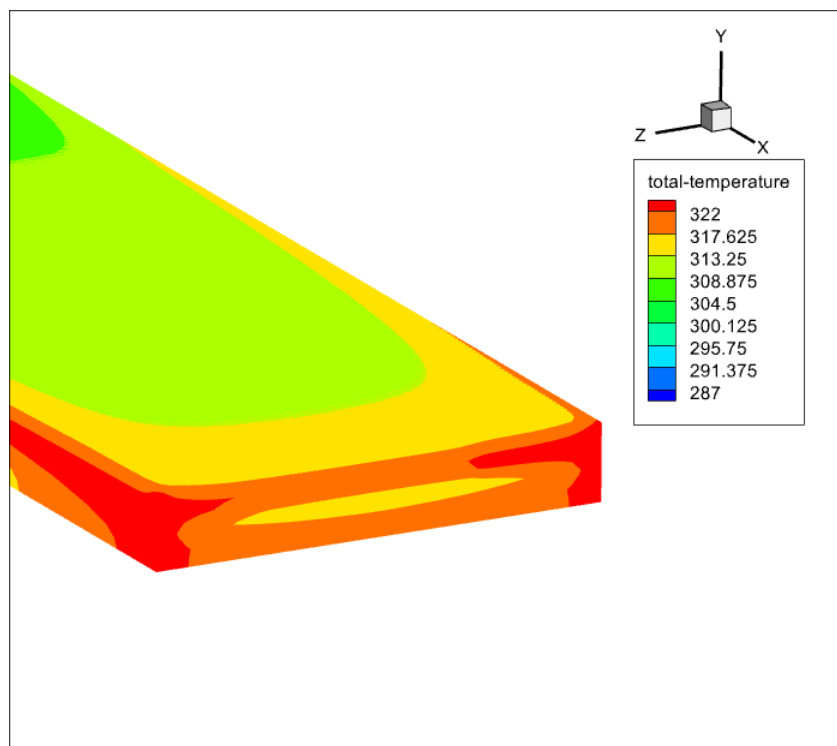


Figure 4.14: outlet at 12:00

4.3 Conclusion

- In this chapter, the results of the numerical simulation of a flat plate air collector have been presented with the goal of studying the thermal behavior of the air flow through the canal and determining its maximum efficiency throughout the day.
- The data from the Adrar region measured experimentally by the URERMS for 5 January 2020 was used because if we guarantee that the performance on 5 January is acceptable as a minimum, then we can always expect a higher performance at other times of the year.
- The problem was approached numerically, based on the finite volume method, using a CFD code (Ansys Fluent).
- Firstly, the tests were carried out using four input speeds (0.3 m/s, 0.1 m/s, 0.08 m/s and 0.05 m/s) taken from the current literature and the external market as being among the most frequently used input speeds.
- After several tests, we have found that the 0.05 m/s velocity is the best air inlet velocity which gives us the best possible performance with a gain of almost 35 degrees at 12:00 which is very satisfying.
- Then, we simulated the behaviour of the collector in different periods of the day with the recently chosen input velocity to check the evolution of the air temperature profile and we saw that the efficiency is between 7 and 35 degrees considering the changes of the temperature and the radiation all along the day.

General conclusion

In this work, we have undertaken a 3D numerical simulation of the thermal fields of a flat plate air collector (solar dryer), in steady state. This study is based on the comparison between different inlet velocities in order to optimise the residence time of the air flowing in a rectangular channel as much as possible, and to have a larger temperature difference at the outlet of the collector. Our numerical model is based on the general equations of conservation of mass (continuity), momentum and energy.

The results obtained from the proposed geometry, materials and dimensions highlight the influence of the inlet velocity on the air temperature, as the heat transfer between the absorbing wall and the tubes will be increasingly important when the air flows slowly. The lower the velocity, the slower the residence time, the higher the exit temperature. It can also be seen that there is an optimal speed for the system, even if the speed is decreased more, the same results are obtained. It can also be seen that the distribution of the thermal field is not homogeneous throughout the system, as the flow is divided over the entire surface of the collector with the air circulation. The lower the velocity, the more energy it receives.

Finally, the study of the two-absorber collector or the addition of several baffles is proposed as a perspective. This solution can set up the homogeneity of the thermal field in the whole system, as there will be only one velocity flowing in the canal.

Bibliography

- [1] URL <https://www.vecteezy.com/vector-art/1142243-diagram-showing-structure-of-the-sun>.
- [2] Yassine BADDOU. Solar thermal systems for domestic water heating applications in residential buildings. efficiency and economic viability analysis of monitored plants. Master's thesis, 2017.
- [3] apparent motion of the sun. URL <https://www.pveducation.org/pvcdrom/properties-of-sunlight/motion-of-the-sun>.
- [4] URL <https://astronomy.swin.edu.au/cosmos/c/Celestial+Sphere>.
- [5] URL <https://www.smithsonianmag.com/science-nature/plan-replace-geographic-coordinates-earth-unique-strings-three-words-180949946/>.
- [6] Ricardo Padilla. Simplified methodology for designing parabolic trough solar power plants. 01 2011.
- [7] URL <https://www.sciencedirect.com/topics/engineering/solar-altitude-angle>.
- [8] URL <https://www.worlddata.info/africa/algeria/sunset.php>.
- [9] URL <http://www.greenrhinoenergy.com/solar/radiation/characteristics.php>.
- [10] URL https://www.researchgate.net/figure/Solar-radiation-potential-in-Algeria-9_fig1_32753174.

- [11] F. Qiu X. Zhang X. Zhao Z. Wang, W. Yang. Solar water heating : From theory, application, marketing and research. *Renewable and Sustainable Energy Reviews*, 2015.
- [12] A. Brahim. Etude de performances d'un capteur solaire plan à eau. Master's thesis, 2016.
- [13] URL www.ladictionnairevisuel.com.
- [14] L. El maimouni N. Hassanain O. Tata Y. Belkassmi, K. Gueraoui. Numerical investigation and optimization of a flat plate solar collector operating with cu/cuo/al2o3–water nanofluids. *Sustainable Energy Technologies and Assessments*, 2020.
- [15] Lee Layton. Solar water heating systems. 2012.
- [16] f. BAUCHE F. SAIDANE. Simulation numérique d'écoulements d'air avec échange de chaleur au sein d'un capteur solaire plan à air. Master's thesis, 2019.
- [17] Maytham Al-Neama and I. Farkas. Utilization of solar air collectors for product's drying processes. *The Journal of Scientific and Engineering Research*, 5: 40–56, 01 2018.
- [18] S. Chaussement. *Statique et dynamique des fluides*, 2011.
- [19] Y. Çengel. *Fluid Mechanics: Fundamentals And Applications*. Tata McGraw Hill Education Private, 2010.
- [20] Bernard J. *Energie solaire calculs et optimisation*. Ellipse Edition Marketing, 2004.
- [21] Sen Z. *Solar energy fundamentals and modeling techniques*. Springer, 2008.
- [22] Alain Ricaud. *Gisement solaire et transferts énergétiques*. Université de CERGY-PONTOISE, 2008.
- [23] B. Mourad. Contribution à l'étude, la simulation et l'analyse des pompes à chaleur assistées par l'énergie solaire. Master's thesis, 2008.

- [24] Y. Jannot. *Thermique solaire*, 2011.
- [25] K. Salima. Effet des paramètres opérationnels sur les performances d'un capteur solaire plan. Master's thesis, 2009.
- [26] SANDALI Messaoud. Etude dynamique et thermique d'un capteur solaire à air à double passe avec milieu poreux. Master's thesis, 2013-2014.
- [27] Modes of heat treatment. URL <https://learnmechanical.com/modes-of-heat-transfer-conduction-convection-and-radiation-pdf/>.
- [28] ABABSA Dalila. Optimisation du rendement d'un capteur solaire par minimisation des pertes convectives. Master's thesis, 2009/2010.
- [29] R. ALILI A. IBERRAKEN. Modélisation mathématique et simulation de capteurs solaires. Master's thesis, 2012.
- [30] H. Schlichting. *Boundary layer Theory, 7th ed.* Springer, 1979.
- [31] O. Reynolds. *On the dynamical theory of incompressible viscous fluids and the determination of the criterion.* the Royal Society of London, 1894.
- [32] I. Paraschivoiu. *Aérodynamique subsonique.* l'École Polytechnique de Montréal (Québec), Canada, 1998.
- [33] S.V Patankar. *Numerical Heat Transfer and Fluid Flow.* CRC Press. New York, 1980.
- [34] B. Djenhi. Contribution à l'étude du transfert de chaleur par convection mixte entre deux plaques parallèles soumises à un chauffage dissymétrique. Master's thesis, 2013.
- [35] I.C. Popa. Modélisation numérique de transfert thermique - méthode des volumes finis. 2002.